Check for updates

The Evolutionary Origin of C_4 Photosynthesis in the Grass Subtribe Neurachninae[1][OPEN]

Roxana Khoshravesh,[a] Matt Stata,[a] Florian A. Busch,[b] Montserrat Saladié,[c] Joanne M. Castelli,[c] Nicole Dakin,[c] Paul W. Hattersley,[c] Terry D. Macfarlane,[c,d] Rowan F. Sage,[a] Martha Ludwig,[c,2] and Tammy L. Sage[a,2,3]

[a]Department of Ecology and Evolutionary Biology, University of Toronto, Toronto, Ontario, Canada, M5S 3B2
[b]Research School of Biology and Australian Research Council Centre of Excellence for Translational Photosynthesis, Australian National University, Acton, Australian Capital Territory 2601, Australia
[c]School of Molecular Sciences, University of Western Australia, Crawley, Western Australia 6009, Australia
[d]Western Australian Herbarium, Department of Biodiversity, Conservation and Attractions, Perth, Western Australia 6983 Australia

ORCID IDs: 0000-0002-1766-8993 (R.K.); 0000-0002-5744-4898 (M.S.); 0000-0001-6912-0156 (F.A.B.); 0000-0002-0088-7233 (M.S.); 0000-0002-7408-1216 (J.M.C.); 0000-0002-7023-9231 (T.D.M.); 0000-0001-6183-9246 (R.F.S.); 0000-0002-0324-7602 (M.L.); 0000-0002-7061-832X (T.L.S.).

The Australian grass subtribe Neurachninae contains closely related species that use C_3, C_4, and C_2 photosynthesis. To gain insight into the evolution of C_4 photosynthesis in grasses, we examined leaf gas exchange, anatomy and ultrastructure, and tissue localization of Gly decarboxylase subunit P (GLDP) in nine Neurachninae species. We identified previously unrecognized variation in leaf structure and physiology within *Neurachne* that represents varying degrees of C_3–C_4 intermediacy in the Neurachninae. These include inverse correlations between the apparent photosynthetic carbon dioxide (CO_2) compensation point in the absence of day respiration (C_*) and chloroplast and mitochondrial investment in the mestome sheath (MS), where CO_2 is concentrated in C_2 and C_4 *Neurachne* species; width of the MS cells; frequency of plasmodesmata in the MS cell walls adjoining the parenchymatous bundle sheath; and the proportion of leaf GLDP invested in the MS tissue. Less than 12% of the leaf GLDP was allocated to the MS of completely C_3 Neurachninae species with C_* values of 56–61 μmol mol^{-1}, whereas two-thirds of leaf GLDP was in the MS of *Neurachne lanigera*, which exhibits a newly-identified, partial C_2 phenotype with C_* of 44 μmol mol^{-1}. Increased investment of GLDP in MS tissue of the C_2 species was attributed to more MS mitochondria and less GLDP in mesophyll mitochondria. These results are consistent with a model where C_4 evolution in Neurachninae initially occurred via an increase in organelle and GLDP content in MS cells, which generated a sink for photorespired CO_2 in MS tissues.

C_4 photosynthesis is a complex trait resulting from the evolutionary reorganization of C_3 leaf anatomy and biochemistry to form an efficient carbon dioxide (CO_2) concentrating mechanism. How the C_4 pathway evolved has been a central issue in plant biology since its discovery over 50 years ago (Downton, 1971). In the past 15 years, phylogenetic studies of C_3 and C_4 species enabled testing of hypotheses concerning when, where, and how the C_4 pathway originated (for example, McKown et al., 2005; Christin et al., 2010, 2011a,b; Kadereit et al., 2012, 2014). Together with physiological and biochemical investigations, these studies support the hypothesis of Monson et al. (1984) that the C_4 pathway arose via a series of innovations that initially enabled plants to refix a large fraction of photorespired CO_2 via the shuttling of Gly from the mesophyll (M) to a sheath of cells surrounding the vascular tissue, where the Gly is decarboxylated (for review, see Sage et al., 2014). The sheath layer is most commonly the bundle sheath (BS) cells, although in some grasses the mestome sheath (MS) cells is where decarboxylation of Gly occurs (Khoshravesh et al., 2016). Associated with the shuttling of Gly is a shift in the expression of the mitochondrial enzyme Gly decarboxylase (GDC) from M cells to the vascular sheath tissue. This requires that the Gly produced in photorespiration diffuses from M to sheath cells for metabolism. Gly shuttling, also known as C_2 photosynthesis, elevates CO_2 levels in the BS two to three times that of M cells, thereby improving Rubisco efficiency (von Caemmerer, 2000; Keerberg et al., 2014). Photosynthetic enhancements in C_2 species are greatest at CO_2 levels below the current atmospheric value of 400 μmol mol^{-1}, supporting a hypothesis that C_2 photosynthesis is a low-CO_2 adaptation that bridges the transition from C_3 to C_4 photosynthesis (Hattersley et al., 1986; Bauwe, 2011; Vogan and Sage, 2012). Consistent with this hypothesis, the C_2 condition is present in more than 40 intermediate species that branch between C_3 and C_4 species on the phylogenetic trees of more than a dozen distinct C_4 lineages (Sage et al., 2014; Lundgren and Christin, 2017; Schüssler et al., 2017).

An important early step proposed for C_2 evolution is the physiological activation of the BS of C_3 species (Gowik and Westhoff, 2011; Sage et al., 2014). Activation of the BS is facilitated by increases in the number and size of mitochondria and chloroplasts and repositioning of

 © 2020 American Society of Plant Biologists. All Rights Reserved.

mitochondria plus a few chloroplasts to the centripetal pole of the BS, possibly to facilitate refixation of some photorespired CO_2 produced in the leaf (Muhaidat et al., 2011; Sage et al., 2013; Voznesenskaya et al., 2013; Khoshravesh et al., 2016). Together, organelle enrichment and repositioning have been termed the "proto-Kranz" phase of early C_4 evolution, and is recognized in close relatives of C_3 and C_2 species in the eudicot genera *Flaveria*, *Heliotropium*, and *Salsola*, and the monocot genus *Steinchisma* (Muhaidat et al., 2011; Sage et al., 2013; Khoshravesh et al., 2016; Schüssler et al., 2017). These observations support a hypothesis that proto-Kranz is a key early step in C_2 evolution. Transition to the C_2 condition occurs with further increases in mitochondrial size and numbers in the BS, increased chloroplast numbers in the BS, and a repositioning of most chloroplasts to the centripetal wall of BS cells (Brown and Hattersley, 1989; Muhaidat et al., 2011; Sage et al., 2013; Khoshravesh et al., 2016). Increases in vein density and BS cross-sectional area can occur in concert with organelle and GDC enrichment in sheath cells of proto-Kranz and C_2 species, and the size and numbers of M cells often decline as well (McKown and Dengler 2007; Muhaidat et al., 2011; Sage et al., 2013; Khoshravesh et al., 2016). Because metabolite flux between M and sheath cells increases as the C_2 and C_4 pathways evolve, increased intercellular transport capacity between these compartments should also increase. C_4 plants are known to have greater frequencies of plasmodesmata (PD) between M and BS cells than that in related C_3 species (Danila et al., 2016, 2018), but it is not known where along the C_3 to C_4 transition the PD frequency increases.

Although research on C_3–C_4 intermediates provides many insights into C_4 evolution, it is largely dominated by results from a handful of species. Over 80% of known intermediates are eudicot, with *Flaveria* species (Asteraceae) in particular dominating research on C_4 origins (Monson and Rawsthorne, 2000; Schulze et al., 2013; Sage et al., 2014). By contrast, only a handful of C_3–C_4 intermediate monocots are known, which is surprising given the predominance of monocot taxa among the C_4 flora. Despite accounting for 78% of all C_4 species, only four of 30 C_4 monocot lineages are known to have C_3–C_4 intermediate species (Hattersley and Stone, 1986; Khoshravesh et al., 2016; Lundgren et al., 2016; Sage, 2016). Of these, the grass genera *Alloteropsis* and *Neurachne* also contain C_4 species, but have only one recognized intermediate species each; *Steinchisma* has five or six species exhibiting C_2 photosynthesis, but it is not close to any C_4 clade (Brown et al., 1983; Aliscioni et al., 2003; Grass Phylogeny Working Group II, 2012). This relatively low number of C_3–C_4 intermediates in the monocots limits investigations into C_4 pathway evolution in grasses and sedges, and constrains development of theoretical models of C_4 evolution. For example, the evolutionary model of Williams et al. (2013) predicts C_4 evolved differently in grasses than eudicots; however, the low number of C_3–C_4 intermediates in the grasses limited parameterization of the monocot algorithms in their model.

The above considerations indicate that identification of additional C_3–C_4 intermediates in grasses and sedges would promote understanding of C_4 evolution in the monocots. To this end, C_3–C_4 intermediates in the grass genera *Alloteropsis* and *Homolepis* have been recently identified (Khoshravesh et al., 2016; Lundgren et al., 2016). Another approach is to re-examine the grass genus *Neurachne* and its allies in the subtribe Neurachninae, where work in the 1980s identified one C_2 species (*Neurachne minor*), two C_4 species (*Neurachne munroi*, and *Neurachne muelleri*—formerly *Paraneurachne muelleri*), and four putative C_3 species (*Neurachne alopecuroidea*, *Neurachne lanigera*, *Neurachne queenslandica*, *Neurachne tenuifolia*; Hattersley et al., 1982, 1986; Hattersley and Roksandic, 1983; Hattersley and Stone, 1986). Subsequent work discovered an additional C_3 species, *Neurachne annularis* (Macfarlane, 2007), whereas *Thyridolepis*, a sister genus in the Neurachninae, contains three putative C_3 species (Prendergast and Hattersley, 1985; Hattersley et al., 1986). This research indicates the potential of the Neurachninae to provide novel insights into C_4 evolution, particularly in the initial transition from a C_3 character state. Work with C_3 relatives of C_4 species describe certain anatomical shifts, such as increases in vein density, that may predispose lineages to evolve C_4 (Muhaidat et al., 2011; Christin et al., 2013; Griffiths et al., 2013; Sage et al., 2013). Similar studies in putative C_3 species of *Neurachne* could also identify anatomical traits that facilitated C_4 evolution in this lineage (Hattersley et al., 1986; Brown and Hattersley, 1989). The Neurachninae also promises unique insights not available in other C_4 lineages, in that the C_4

[1]This work was supported by the Australian Research Council (Discovery Grant no. DP130102243 to M.L., R.F.S., and T.L.S.), the Canadian Natural Science and Engineering Research Council (grants no. RGPIN-04878-2015 to T.L.S. and no. RGPIN-2017-06476 to R.F.S.), the Australian Government through the Australian Research Council Centre of Excellence for Translational Photosynthesis (to F.A.B.), and a Queen Elizabeth II Graduate Scholarship in Science and Technology (to Ma.S.).

[2]Senior authors.

[3]Author for contact: tammy.sage@utoronto.ca

The author responsible for distribution of materials integral to the findings presented in this article in accordance with the Journal policy described in the Instructions for Authors (http://www.plantphysiol.org) is: Martha Ludwig (martha.ludwig@uwa.edu.au).

R.K. and T.L.S. conducted the microscopy and immunolocalizations; F.A.B. and R.F.S. conducted leaf gas exchange; J.M.C. and Mo. S. conducted the immunoblots; Mo.S. conducted the reverse transcription-quantitative PCR analyses; Ma.S. and R.K. conducted phylogenetic trait reconstruction; P.W.H., T.D.M., R.F.S., and M.L. collected the species, which were grown and maintained by M.L.; M.L. generated the anti-GLDP antibody; T.L.S., N.D., and R.K. sampled all materials for microscopy; the design and management of the project was jointly shared by M.L., T.L.S., R.F.S., and R.K.; funding was acquired by M.L., R.F.S., and T.L.S.; the article was written by R.F.S., T.L.S., Ma.S., R.K., and M.L.

[OPEN]Articles can be viewed without a subscription.

www.plantphysiol.org/cgi/doi/10.1104/pp.19.00925

Neurachne species exhibit a distinct form of Kranz anatomy termed "Neurachneoid," where a suberized MS is the site of CO_2 concentration (Dengler and Nelson, 1999; Edwards and Voznesenskaya, 2011). These cells are in turn surrounded by an outer sheath of parenchyma cells considered to have low photosynthetic activity (Hattersley et al., 1982, 1986). The combined resistance of the suberized MS wall and the parenchymatous sheath (PS) could have profound implications for how C_4 evolved in *Neurachne*, and other grass lineages where CO_2 is concentrated in the MS, such as *Alloteropsis* (Lundgren et al., 2019). In addition, it is now possible to evaluate evolutionary hypotheses in the Neurachninae with the publication of a species-level molecular phylogeny (Christin et al., 2012). The Neurachninae clade is young (<10 million years old), increasing the likelihood that unknown intermediate traits persist (Christin et al., 2012). Both C_4 *Neurachne* species use the NADP-malic enzyme subtype of C_4 photosynthesis (Hattersley and Stone, 1986; Moore and Edwards, 1989), which the molecular phylogeny indicates were independently acquired (Christin et al., 2012).

To develop a more comprehensive understanding of the tissue and cellular changes during C_4 grass evolution, this study re-examined the physiological and structural diversity of nine species of the Neurachninae subtribe using leaf gas exchange, leaf anatomical and ultrastructural studies, and immunolocalization of the P-subunit of GDC (GLDP) and Rubisco large subunit (LSU). Structural assessments include quantitative analyses of MS versus M cell dimensions, organelle size and numbers, interveinal distance (IVD), and the relative contribution of MS, PS, and M tissue to the leaf volume. PD frequencies between MS and PS cells and between PS and M cells were also evaluated to assess potential changes in intercellular transport capacities along the evolutionary transition. Gas exchange analysis allowed us to relate modifications in leaf structure to physiological performance, with the parameter C_* (the apparent CO_2 compensation point in the absence of day respiration) being our main index of photorespiratory CO_2 refixation after Gly shuttling (Sage et al., 2013). We used the recent phylogeny of Neurachninae (Christin et al., 2012) to interpret observed trait shifts in an evolutionary context.

RESULTS

Leaf Gas Exchange

At 32°C, the response of net CO_2 assimilation rate (A) to intercellular CO_2 partial pressure (C_i) for *N. muelleri* and *N. munroi* was typical of C_4 plants, showing a CO_2 compensation point (Γ) near 0 μmol mol^{-1}, a steep initial slope, and a CO_2 saturation point below a C_i of 400 μmol mol^{-1} (Fig. 1; Table 1). *N. alopecuroidea*, *N. queenslandica*, and *Thyridolepis mitchelliana* exhibited A/C_i responses typical of C_3 photosynthesis, with $\Gamma > 60$ μmol mol^{-1}, a low initial slope relative to the C_4 species, and a CO_2 saturation point exceeding 1,000 μmol m^{-2} s^{-1} (Fig. 1; Table 1; A/C_i curves not shown for *T. mitchelliana*). We consider these three species "completely" C_3 plants to distinguish them from *N. annularis* that is functionally C_3 although it exhibits some intermediate structural characteristics. In *N. annularis*, Γ was C_3-like at 65 μmol mol^{-1} at 32°C. The C_2 species *N. minor* exhibited responses to C_i that were intermediate between the C_3 and C_4 responses, with a Γ of 16 μmol mol^{-1} at 32°C. In *N. lanigera*, Γ was 56 μmol mol^{-1} at 32°C, and 58 μmol mol^{-1} at 35°C; this latter Γ value was significantly less than in the *Neurachne* species that exhibi C_3-like Γ values at 35°C. Carboxylation efficiency was statistically the same in all non-C_4 species of Neurachninae that were examined at 32°C (Table 1).

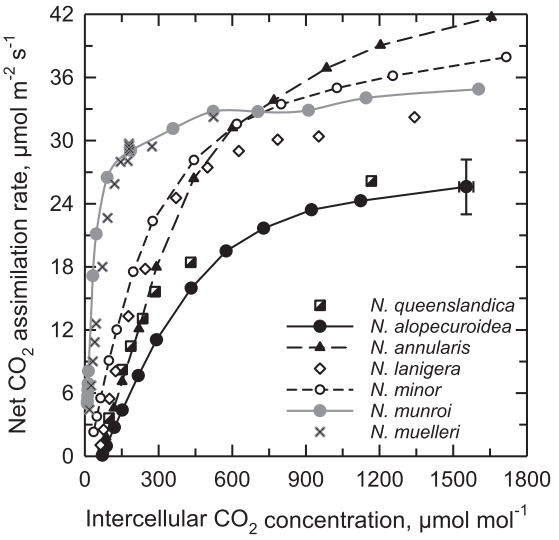

Figure 1. The response of net CO_2 assimilation rate to variation in intercellular CO_2 concentration in seven species of *Neurachne* at 32°C. Each curve is a single representation of three to five measurements per species. The highest CO_2 assimilation rate for *N. alopecuroidea* also presents ± SE to show a typical SE range.

C_* was measured at 35°C to enhance photorespiration and the ability to resolve differences between C_3, proto-Kranz, and C_2 species (Fig. 2; Table 1). In C_4 plants, C_* cannot be measured due to C_4 metabolism, so Γ at high light was measured instead (for convenience in comparing species, C_4 Γ is treated as equivalent to C_* in the discussion of results). As shown in Figure 2, there is good convergence of the initial slopes of the A/C_i responses upon a common intercept at all light intensities (*N. alopecuroidea*, *N. annularis*, and *N. lanigera*), or light intensities at <500 μmol m^{-2} s^{-1} (*N. minor*). For *N. alopecuroidea*, *N. queenslandica*, *N. annularis*, and *N. lanigera*, all plots of the y-intercept versus the initial slope of the A/C_i response closely fit a linear response, with the slope of the response being similar for each species (Supplemental Fig. S1). For *N. minor*, by contrast, only the values <500 μmol m^{-2} s^{-1} fit a linear response; the value at high light did not correspond to the linear response due to a shift in the high-light A/C_i response to lower C_i (Supplemental Fig. S1). Mean C_*

Table 1. *Summary of leaf gas exchange results for Neurachninae species*

Letters indicate common statistical groups at $P < 0.05$ (one-way ANOVA followed by a Tukey's posthoc test). Mean ± SE, n = 3–9 except for *N. munroi* where n = 2 at 35°C. ND, not determined.

Species	C_*, μmol μmol mol^{-1}	Γ at Saturating Light, μmol mol^{-1}		Carboxylation Efficiency μmol m^{-2} s^{-1}	
	35°C	32°C	35°C	32°C	35°C
T. mitchelliana	61.1 ± 0.5 a	ND	62.4 ± 0.5 c,d	ND	0.22 ± 0.02 b
N. alopecuroidea	60.9 ± 2.0 a	71.1 ± 2.3 a	78.5 ± 2.0 a	0.05 ± 0.00 b	0.05 ± 0.01 d
N. queenslandica	55.9 ± 0.7 a	62.8 ± 1.0 a,b	69.2 ± 1.0 b	0.10 ± 0.02 b	0.08 ± 0.00 c,d
N. annularis	54.4 ± 0.7 a	65.0 ± 2.7 a,b	66.9 ± 1.0 b,c	0.09 ± 0.01 b	0.13 ± 0.00 c
N. lanigera	44.1 ± 0.9 b	55.6 ± 0.9 b	58.1 ± 1.7 d	0.13 ± 0.01 b	0.12 ± 0.03 c,d
N. minor	16.7 ± 0.9 c	15.6 ± 4.6 c	14.3 ± 1.2 e	0.11 ± 0.01 b	0.09 ± 0.02 c,d
N. munroi	ND	2.0 ± 0.4d	1.7 ± 0.3 f	0.50 ± 0.13 a	0.51 ± 0.03 a
N. muelleri	ND	0.3 ± 0.0d	ND	0.27 ± 0.02 b	ND

values at 35°C for *T. mitchelliana*, *N. alopecuroidea*, and *N. queenslandica* were C_3-like, being 56 μmol mol^{-1} to 61 μmol mol^{-1} (Table 1). For *N. annularis*, C_* was 54 μmol mol^{-1}, which is statistically equivalent to the C_3 group; in *N. lanigera*, C_* was 44 μmol mol^{-1}, significantly less than the values of C_3 Neurachninae species (Table 1). C_* for *N. minor* was 17 μmol mol^{-1}, a typical value for C_2 species (Khoshravesh et al., 2016). Because C_* reflects the magnitude of photorespiratory CO_2 refixation (Busch et al., 2013; Sage et al., 2013), the observed C_* values can be used to evaluate relationships between photosynthetic physiology and the underlying leaf structure.

Leaf and Cellular Architecture

The leaf architecture of Neurachninae species varies dramatically between the C_3 and C_4 phenotypes, in a manner that is consistent with differences between these photosynthetic pathways in many monocot and eudicot clades where the C_4 pathway evolved (Hattersley and Watson, 1975; Hattersley, 1984; Dengler and Nelson, 1999; Christin et al., 2013). Specifically, IVD, the ratio of M to MS tissue area in a cross section, and the M cell number between PSs of minor veins decreases from C_3 to C_4 species (Fig. 3, A–C; Supplemental Table S1). In species with C_* values > 40 μmol mol^{-1}, MS cells have a smaller cross-sectional area (<45 μm^{-2}) in comparison to the larger (>100 μm^{-2}) MS cells in species where $C_* < 20$ μmol mol^{-1} (Fig. 3A; Supplemental Table S1). This increase in cross-sectional area of the MS cells in *Neurachne* as C_* declines mirrors changes in BS cell area and width (W) in planar cross sections from many clades where C_4 photosynthesis evolved, leading to the general view that C_4 species have more voluminous BS or MS cells relative to their C_3 relatives (Dengler and

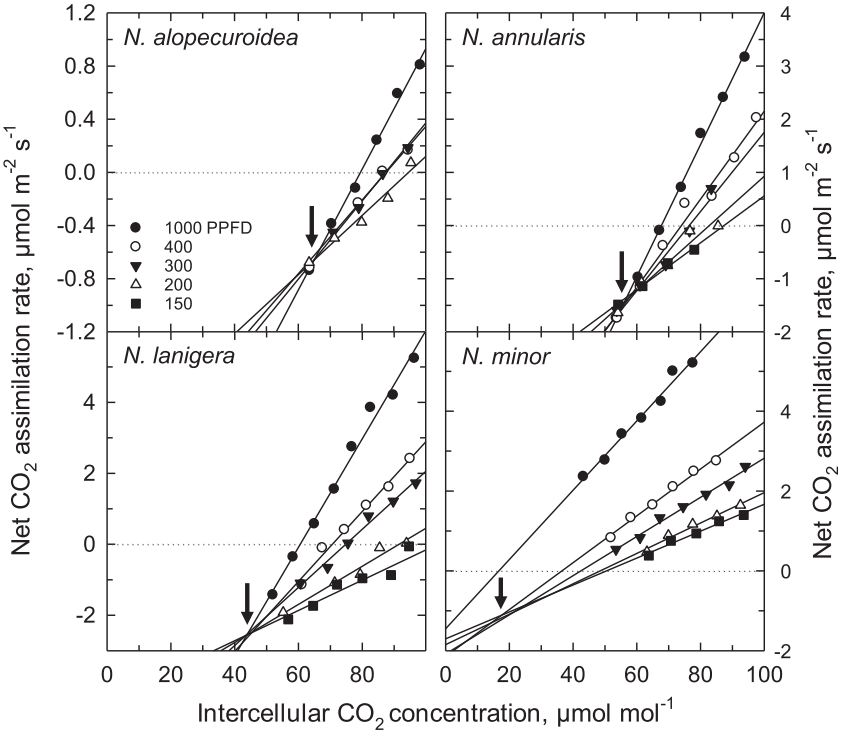

Figure 2. The response of net CO_2 assimilation rate to variation in intercellular CO_2 concentration (C_i) at <100 μmol CO_2 mol^{-1} air in four species of *Neurachne* at 35°C and four to five light intensities. The C_i where the curves intercept is an estimate of C_*, the apparent CO_2 compensation point in the absence of day respiration (arrows). Curves are representative of three to eight A/C_i plots per species. Note the y axis range varies between the graphic representations. PPFD, photosynthetic photon flux density in μmol photons m^{-2} s^{-1}.

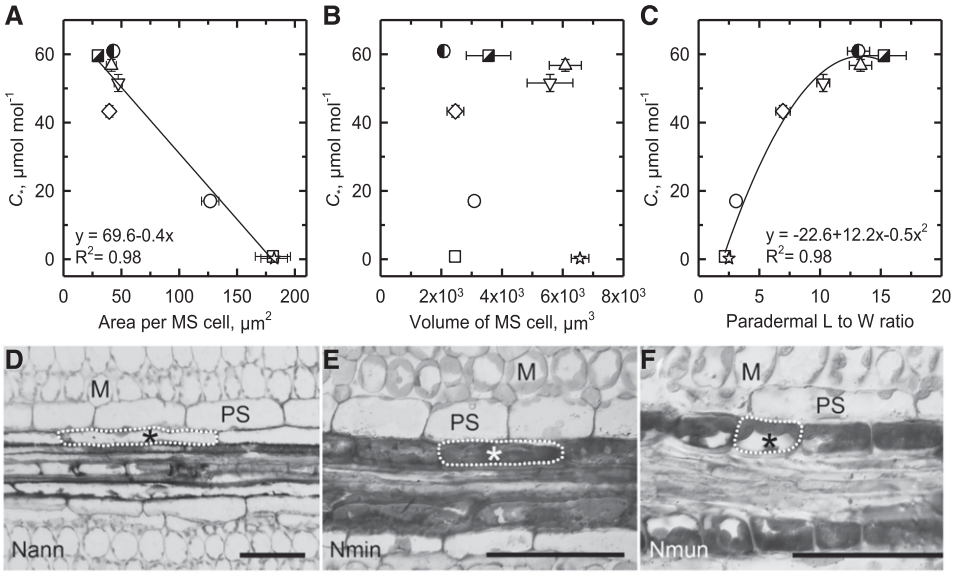

Figure 3. The relationship between C_* and dimensions of MS cells. A, MS cell area in planar cross section. B, MS cell volume. C, MS cell L:W in a paradermal section in eight species of Neurachnineae. Values were determined from planar cross sections of TEM images (A and B). Values were determined from light microscopic images of planar paradermal sections (C). Mean ± SE; n = 3 plants per species; 10 images per plant. Significant regressions at $P \leq 0.05$ are shown. *N. alopecuroidea* (◑), *N. annularis* (▽), *N. lanigera* (◇), *N. minor* (○), *N. munroi* (□), *N. muelleri* (☆), *N. queenslandica* (△), and *T. mitchelliana* (◪). See Supplemental Table S1 for values and statistical tests. D to F, Paradermal view of vascular sheath cells. Nann, *N. annularis*; Nmin, *N. minor*; Nmun, *N. munroi*. Single MS cells are outlined (dashed line). Scale bars = 50 µm; *, MS, M, and PS.

Nelson, 1999; Christin et al., 2013; Williams et al., 2013). To further evaluate changes in MS size and shape during C_4 evolution, we estimated MS cell volume by multiplying the cross-sectional area times the cell length (L) in a paradermal section, which is possible because MS and BS cells in grasses are cylindrical in shape (Leegood, 2008). Our estimated volume of MS cells does not support the common view that MS cells become larger during C_4 evolution. No increase in MS volume was observed in C_4 relative to C_3 or intermediate Neurachninae species and there is no relationship between MS cell volume and C_* (Fig. 3B; Supplemental Table S1). This is because MS cells decrease in L (the dimension along the proximo-distal axis parallel to the veins in grass leaves) and increase in W (the dimension along the medio-lateral axis perpendicular to grass veins) as C_* declines (Fig. 3, C–F). The MS cells in the C_3 species such as *N. alopecuroidea* are long and relatively thin (high L:W), whereas in C_4 species such as *N. munroi*, they are short and wide as shown by changes in L:W that decline from near 15 in C_3 species to <5 in C_4 species (Fig. 3, D–F; Supplemental Table S1). *N. lanigera* and *N. minor* have intermediate L:W, reflecting a transition from the C_3- to C_4-type MS cell. A second-order regression predicted 98% of the variation in this relationship (Fig. 3C). These morphological changes result in an increase in MS cell number along the length of the vascular strands (Fig. 3, D–F).

Increased MS cell width, as well as reductions in interveinal M cell number, contribute to modifications in the percent of leaf tissue occupied by MS and M tissue in C_3 compared to C_2 and in turn C_4 species (Fig. 4, Supplemental Table S1; Supplemental Fig. S2). Whereas <10% of the cross-sectional area of photosynthetic tissue is occupied by MS in the C_3 species with $C_* > 50$ µmol mol^{-1}, MS tissue accounts for >20% of the leaf cross-sectional area in species with $C_* < 20$ µmol mol^{-1} (Fig. 4A). The reduction in C_* from C_3 to C_2 to C_4 species was also associated with a decline in the percent of M tissue in a cross section, from >80% of the cross-sectional image area at a $C_* > 60$ µmol mol^{-1} to ~60% at a $C_* < 20$ µmol mol^{-1} (Fig. 4C). As M:MS, IVD, and interveinal M cell number decline, so does C_* in a linear manner, with each regression having a significant slope (Fig. 4, D–F). No relationship was observed between percentage of PS tissue area and C_* (Fig. 4B).

The allocation of chloroplasts to MS tissue also increases as C_* declines from C_3 to the C_4 values in Neurachninae (Figs. 5 and 6; Supplemental Table S2; Supplemental Fig. S3). In the C_3 species *T. mitchelliana*, *N. queenslandica*, *N. alopecuroidea*, and *N. annularis*, <5% of the chloroplast cross-sectional area within leaf photosynthetic tissue occurs in the MS (Figs. 5, A and B, and 6A). This fraction rises to >9% and 20% in *N. lanigera* and *N. minor*, respectively, and to near 50% in the C_4 species (Figs. 5, C and D, and 6A; Supplemental Table S2). Increases in chloroplast size and number within the MS protoplast contribute to greater chloroplast investment in MS tissue of intermediate and C_4 species (Figs. 5, E and F, and 6A; Table 2). Enhanced mitochondrial numbers and size contribute to greater mitochondrial investment in MS tissue as C_* declines from C_3 to C_2

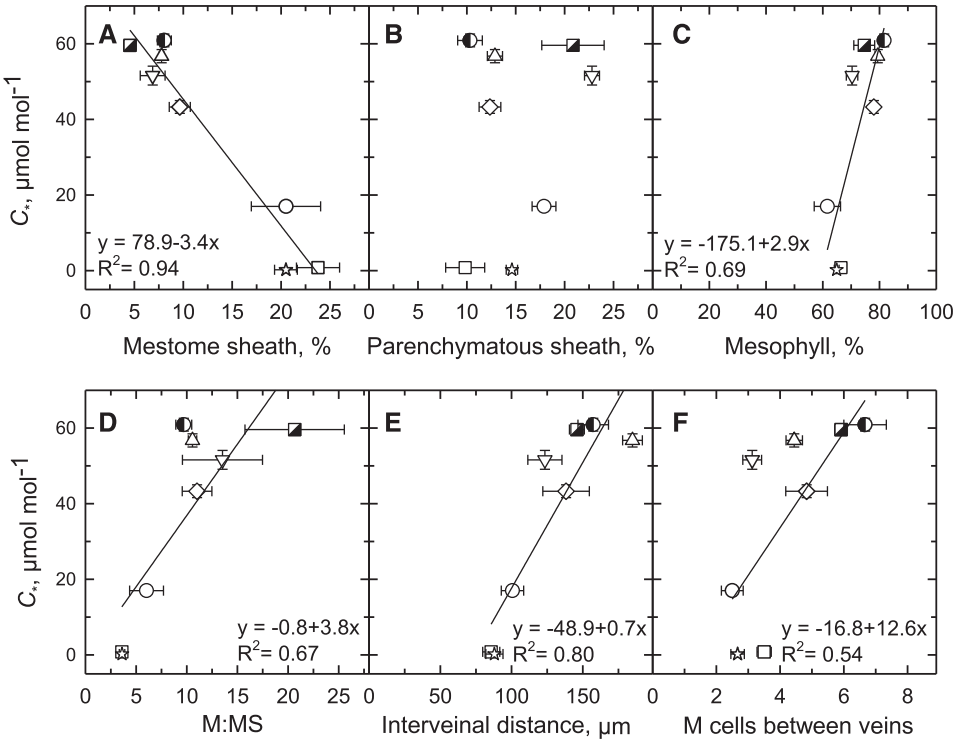

Figure 4. The relationship between leaf structural parameters and C_* in eight Neurachninae species. Values determined from light microscopic images of planar cross sections. Percent tissue values were calculated as the area of a given tissue in a leaf image divided by the sum of the areas of MS, PS, and M tissues in the same image, times 100% (Supplemental Fig. S2). A, Percent of image area composed of MS tissue. B, Percent of image area composed of PS tissue. C, Percent of image area comprised of M tissue. D, The ratio of M tissue area to MS tissue area in planar cross section. E, Mean distance between veins. F, The number of M cells between veins. Mean ± SE; $n = 3$ plants per species; 10 images per plant. See Supplemental Table S1 for mean values and statistical tests. Significant linear regressions at $P \leq 0.05$ are shown. *N. alopecuroidea* (◑), *N. annularis* (▽), *N. lanigera* (◇), *N. minor* (○), *N. munroi* (□), *N. muelleri* (☆), *N. queenslandica* (△), and *T. mitchelliana* (◪).

species (Figs. 5, A–D, and 6B; Table 2; Supplemental Table S2; Supplemental Fig. S3). In *N. lanigera* and *N. minor*, >40% and 60%, respectively, of the mitochondrial cross-sectional area within leaf photosynthetic cells occurs in the MS (Figs. 5, C and 5D, and 6B; Supplemental Table S2). In the MS of the C_4 species, mitochondrial investment is lower than in C_2 species, due to a reduction in mitochondrial numbers (Figs. 5, E and F, and 6B; Table 2; Supplemental Table S2).

Immunodetection of GLDP and Rubisco LSU

To quantify GLDP in tissues of the Neurachninae species, a polyclonal antiserum was generated against a highly conserved 16-amino acid-peptide present in eudicot and monocot GLDP isoforms. The specificity of the antiserum was determined by immunoblot analysis of *Neurachne* leaf extracts after denaturing PAGE (Supplemental Fig. S4A). A single polypeptide band of ~98 kD corresponding to the molecular mass of GLDP was detected in all *Neurachne* leaf extracts (Supplemental Fig. S4B). The labeling shows lower content of GLDP protein, on a total protein basis, in leaves of the C_4 species *N. munroi* and *N. muelleri* relative to that in leaves of *N. annularis*, *N. queenslandica*, *N. lanigera*, and *N. minor* (Supplemental Fig. S4B). Less intense GLDP labeling in *N. alopecuroidea* extracts is due to protein degradation, which is inherently high in this species compared with other Neurachninae even in the presence of protease inhibitors, and is evident in the Coomassie-stained gel (Supplemental Fig. S4A). The relative abundance of transcripts encoding GLDP was generally greater in the C_3 and C_2 species than in the C_4 species (Supplemental Fig. S4D), reflecting the relative patterns of GLDP protein in the leaves of the various species (Supplemental Fig. S4B).

When the anti-GLDP serum was used to label sections of Neurachninae leaves, the density of GLDP labeling per protoplast planar area increased in MS cells as C_* declined from near 60 μmol mol^{-1} in completely C_3 species to the 44 μmol mol^{-1} observed in *N. lanigera* (Table 2). The density of GLDP labeling per protoplast area in the MS cells of *N. annularis* was double that of *N. alopecuroidea*, which had the highest density of GLDP gold labeling per protoplast area in the MS cells of the three completely C_3 species (2.92 versus 1.45 gold particles μm^{-2}; Table 2). The density of GLDP labeling per

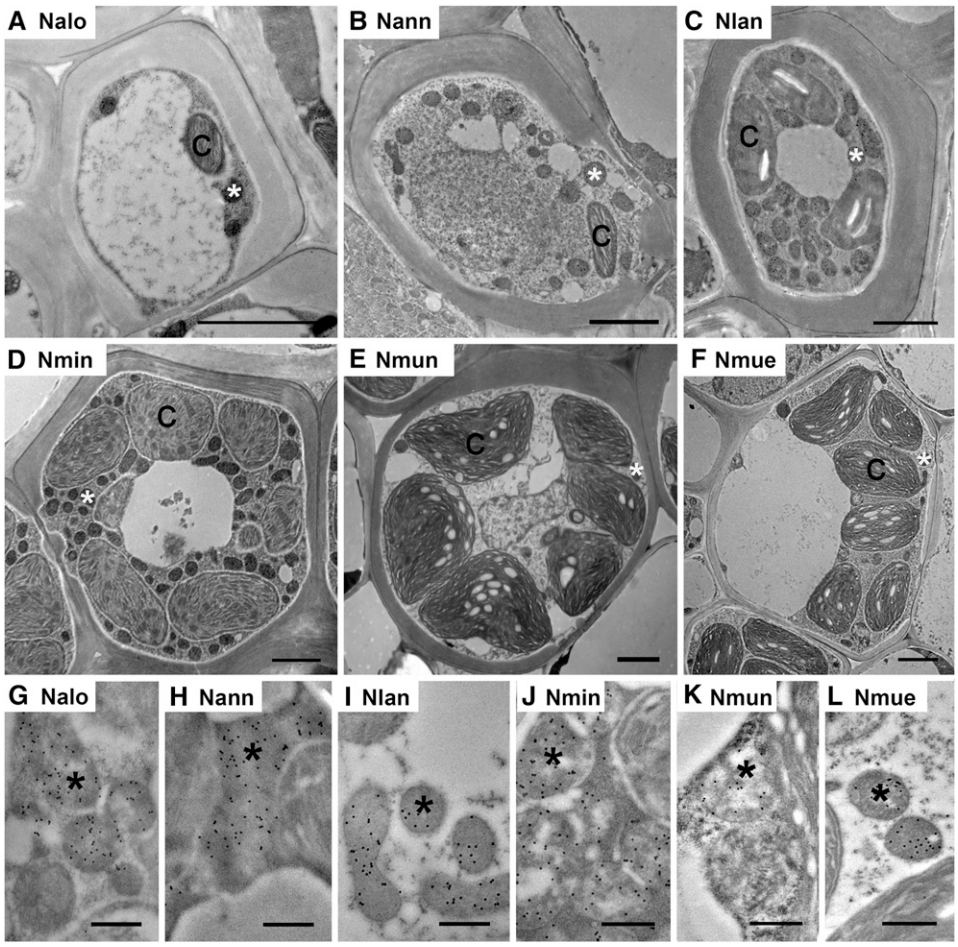

Figure 5. TEM images of MS cells of six *Neurachne* species. A to F, Low magnification images illustrating ultrastructure. G to L, Immunogold labeling of GLDP in MS mitochondria. Immunogold labeling of GLDP is indicated by black dots in mitochondria. Nalo, *N. alopecuroidea*; Nann, *N. annularis*; Nlan, *N. lanigera*; Nmin, *N. minor*; Nmun, *N. munroi*; Nmue,*N. muelleri*; C, chloroplast; *, mitochondrion. Scale bars = 2 μm (A–F); 500 nm (G–L).

protoplast area in the MS cells was almost three times higher in *N. lanigera* and *N. minor* than the highest completely C_3 mean (4.4 versus 1.45 particles μm^{-2}; Table 2). These differences largely reflected the increase in mitochondrial area in the protoplast of MS cells of *N. annularis*, *N. lanigera*, and *N. minor* relative to the completely C_3 species, because the amount of GLDP labeling per mitochondrion area did not consistently differ between the Neurachninae photosynthetic types (Fig. 5; Table 2). GLDP labeling per planar area of MS protoplasts was low in the C_4 species relative to *N. lanigera* and *N. minor*, which reflects both low mitochondrial area in the C_4 MS and reduced GLDP labeling per mitochondrion (Fig. 5, C–F and I–L; Table 2). Low mitochondrial area in the MS or BS cells is commonly observed in NADP-ME species, which include *N. muelleri* and *N. munroi* (Hattersley et al., 1986; Sage et al., 2014). *T. mitchelliana* exhibited very low amounts of GLDP labeling in the mitochondria of MS cells, which reflects low mitochondrial cross-sectional area and low GLDP content per mitochondrion (Table 2). Along with low values of chloroplast area in the MS cells, these results indicate the MS cells of C_3 *T. mitchelliana* are photosynthetically inactive compared to those of the other completely C_3 *Neurachne* species, which have higher organelle content and GLDP levels.

In contrast to the patterns observed in the MS cells of the completely C_3 species, the density of GLDP labeling per protoplast and mitochondrial planar area declined in M cells as C_* declined, such that GLDP labeling of the M cells is negligible in the C_4 species and *N. minor* (Table 2; Supplemental Fig. S5). The near-absence of GLDP labeling in M cells of *N. minor* corresponds to its robust C_2 cycle as indicated by the low C_* of 17 μmol mol^{-1} at 35°C. GLDP content per protoplast planar area also declined with C_* in the PS cells (Fig. 6; Table 2). The increase in GLDP labeling in the MS cells coupled with its reduction in the M and PS cells results in an increase in the fraction of leaf GLDP labeling present in the MS tissue, and this correlates with a reduction in C_* in the Neurachninae (Fig. 6C; Supplemental Table S2). The quantification of immunogold particles indicated 100% of the leaf GLDP was present in the MS tissue of *N. minor*, whereas 67% and 22% of leaf GLDP was present in the MS tissue in *N. lanigera* and *N. annularis*, respectively. In the MS tissue of the completely C_3 species *N. alopecuroidea*, *N. queenslandica*, and *T. mitchelliana*, the fraction of GLDP labeling was <22%. In the two C_4 species, all of the leaf GLDP labeling detected was in MS tissue (Fig. 6C; Supplemental Table S2).

Strong labeling of an ~56-kD polypeptide, corresponding to the LSU of Rubisco, was detected in all

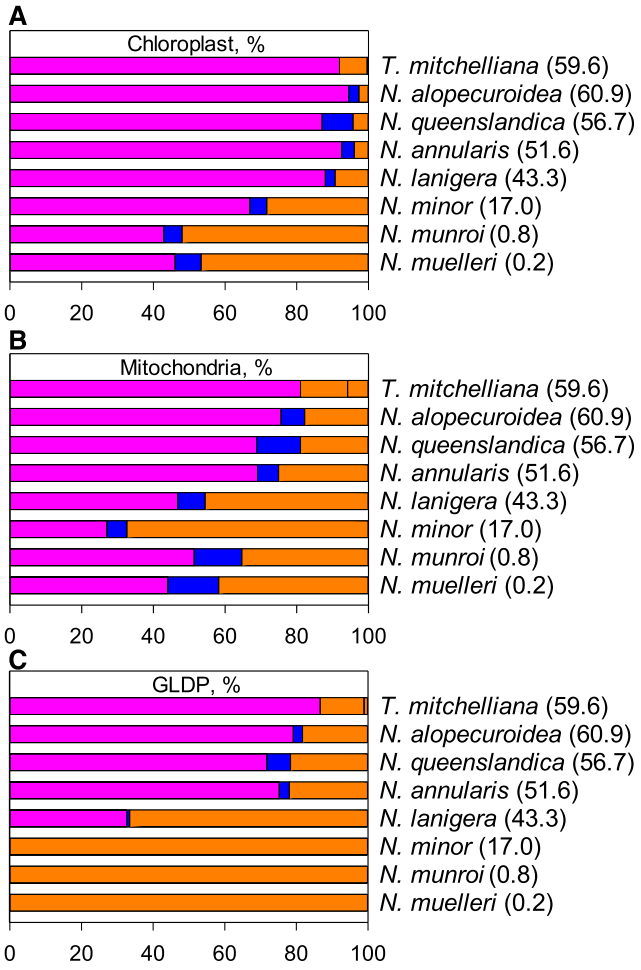

Figure 6. The allocation of organelles and GLDP among leaf tissue types. A, Chloroplast. B, Mitochondria. C, GLDP among M (magenta, left bar), PS (blue, middle bar), and MS (orange, right bar) tissues in eight species of Neurachnineae. Values in parentheses represent mean C_* values for each species. $n = 3$ plants per species; 10 images per plant. See Supplemental Table S2 for mean values, statistical tests, and quantification procedure.

Neurachninae species when blots of total leaf protein were labeled with an anti-Rubisco LSU antiserum (Supplemental Fig. S4C). Immunolabeling of the Rubisco LSU was detected in chloroplasts of MS and PS cells in all species, and in M cells of all species except the C_4 *N. munroi* and *N. muelleri* (Supplemental Figs. S6–S8). Rubisco LSU immunolabeling in the PS cells was very low in *N. annularis*, *N. lanigera*, *N. minor*, and the two C_4 species. The absence of Rubisco LSU immunolabeling in M cells of *N. munroi* and *N. muelleri* reflects their use of the C_4 pathway.

PD Frequency

Because an increase in the frequency of PD between M and BS cells is characteristic of C_4 relative to C_3 species (Danila et al., 2016, 2018), we examined PD frequency in the MS, PS, and M walls of the different Neurachninae species to evaluate the hypothesis that PD frequency increases in C_2 species to accommodate the increased flux of photorespiratory metabolites among M, PS, and MS cells. The PD frequency at the MS–PS cell wall boundary significantly increases in Neurachninae species when C_* declines from >60 μmol mol^{-1} to <15 μmol mol^{-1} (Fig. 7A; Supplemental Table S3). The regression between PD frequency in the MS–PS wall and C_* predicts 98% of the variation in the relationship. A significant inverse relationship was also present between PD frequency in the PS–M wall and C_*, with an R^2 of 0.74 (Fig. 7B; Supplemental Table S3). When species means were pooled by photosynthetic type, the C_4 mean for PD frequency in the MS–MS cell wall was greater than the C_3 mean ($P \leq 0.05$).

Phylogenetic Principal Component Analysis

Of the many anatomical, cellular, and GLDP traits examined (Table 2; Supplemental Tables S1–S3), 13 are significantly correlated with C_* (Supplemental Table S4). These 13 traits include IVD, MS L:W, the allocation of mitochondria, chloroplasts, and GLDP labeling in MS versus M tissue, as well as PD frequency between MS–PS, MS–MS, and PS–M cells. The pair comparison of phylogenetic independent contrasts between these 13 variables exhibited similar significance of correlation (Supplemental Fig. S9). To correct for phylogenetic signal, a phylogenetic principal component analysis (pPCA) was performed using the traits that exhibited high correlation in species values and the corresponding phylogenetic contrasts for C_* values (Fig. 8; Revell, 2009, 2012). Five of seven principal components identified by pPCA had eigenvalues > 0.1 (Supplemental Table S5), and pPC1 and pPC2 explained 79% and 12% of variance, respectively (Fig. 8; Supplemental Table S5). In the pPCA plot, the values for *N. annularis* place it near the completely C_3 species on the right-hand side of the pPC1 axis, but displaced toward the C_4 species along pPC1. C_4 species cluster on the left side of the pPC1 axis, whereas values for *N. lanigera* and *N. minor* are spaced between the C_3 and C_4 values along the pPC1 but shifted upwards along pPC2 axis relative to the C_3 and C_4 species (Fig. 8). pPC1 is negatively correlated with parameters associated with the MS tissue, and positively correlated with M tissue-related parameters. Species with C_3, incomplete C_2, complete C_2, and C_4 photosynthesis spread from right to left, respectively, along pPC1 in response to reductions in chloroplast, mitochondria, and GLDP investment in M tissue, and to increases in chloroplast, mitochondria, and GLDP in MS tissue (Fig. 8; Supplemental Table S6). pPC2 is negatively correlated with M tissue mitochondrial number and positively correlated with MS tissue mitochondrial number. The correlation of pPC2 with the remaining variables is negligible (<0.3). A linear model with C_* as the response of the five first pPCs indicates that pPC1 significantly predicts the C_* values

Table 2. *Organelle parameters and gold density labeling of GLDP in tissues of Neurachninae species*

Values are from planar cross sections of TEM images. Mean ± SE; $n = 3$ plants per species; 10 images per plant. Values followed by the same letter in each row are not significantly different ($P \geq 0.05$) using a Tukey's post hoc test for normally distributed data (*) and a Games–Howell test for all other data. See Supplemental Table S3 for peroxisome area per protoplast area. PK, Proto-Kranz phenotype.

Parameter by Tissue Type	Completely C_3 Species			C_3 PK	Modest C_2[a]	C_2 Species[b]	C_4 Species	
	T. mitchelliana	*N. queenslandica*	*N. alopecuroidea*	*N. annularis*	*N. lanigera*	*N. minor*	*N. munroi*	*N. muelleri*
Area per chloroplast, μm^2								
Mestome sheath	0.6 ± 0.2 a	4.1 ± 0.6 a	3.4 ± 0.4 a	3 ± 0.3 a	3.5 ± 0.3 a	8.3 ± 0.8 b	19.2 ± 1 b	8.6 ± 0.5 b
Mesophyll	5.4 ± 0.4 a	8.9 ± 0.7 b	6.4 ± 0.4 a	7.5 ± 0.4 a	6.8 ± 0.4 a	6.7 ± 0.3 a	10.6 ± 0.9 b	6.6 ± 0.4 a
Parenchymatous sheath	3.5 ± 0.5 a,b	4.8 ± 1 b	2.8 ± 0.3 a	2.9 ± 0.2 a	2.3 ± 0.3 a	3.7 ± 0.3 a,b	7.7 ± 0.4 c	3.4 ± 0.2 a,b
Area per mitochondrion, μm^2								
Mestome sheath	0.08 ± 0.02 a	0.21 ± 0.04 a	0.22 ± 0.02 a	0.3 ± 0.03 b	0.3 ± 0.02 b	0.36 ± 0.02 b	0.42 ± 0.02 c	0.32 ± 0.02 b
Mesophyll	0.24 ± 0.06 a,b	0.31 ± 0.03 b	0.21 ± 0.03 a	0.28 ± 0.02 a,b	0.25 ± 0.02 a,b	0.21 ± 0.02 a	0.37 ± 0.03 c	0.25 ± 0.02 a,b
Parenchymatous sheath	0.15 ± 0.02 a	0.21 ± 0.02 a	0.15 ± 0.01 a	0.16 ± 0.01 a	0.18 ± 0.01 a	0.21 ± 0.03 a	0.37 ± 0.05 b	0.21 ± 0.03 a
Chloroplast area/protoplast area, %								
Mestome sheath	1.4 ± 0.4 a	12.9 ± 2.7 b	12.2 ± 2.9 b	16.4 ± 1.9 b	27.5 ± 2.8 c	46.5 ± 3.3 d	74.2 ± 2.4 e	38.7 ± 1.7 d
Mesophyll	15.7 ± 1.2 a,b	21.6 ± 1.9 a,b	38.2 ± 2.4 d	33.4 ± 2.2 c,d	24.4 ± 1.9 b,c	21.4 ± 1.8 a,b	18.8 ± 1.9 a,b	11.4 ± 1.0 a
Parenchymatous sheath	4.7 ± 0.8 a,b	16.3 ± 3.8 c	8.0 ± 1.0 c	4.2 ± 0.5 a	4.7 ± 0.6 a,b	6.5 ± 0.7 a,b,c	11.0 ± 1.0 c	7.3 ± 0.8 b,c
Chloroplast #/protoplast area, $\mu m^{-2} \times 10^{-3}$								
Mestome sheath	20.0 ± 4.7 a	32.4 ± 7.2 a,b	34.8 ± 7.5 a,b	56.3 ± 5.9 b,c	84.0 ± 8.7 c	62.6 ± 4.9 b,c	41.9 ± 2.6 b	47.8 ± 2.3 b
Mesophyll*	29.9 ± 2.2 c	26.8 ± 1.8 c,b	58.4 ± 3.3 a	45.3 ± 2.6 b	36.7 ± 3.2 c	30.7 ± 1.9 c	19.0 ± 1.6 d,e	17.5 ± 1.1 e
Parenchymatous sheath	13.1 ± 1.6 a	33.3 ± 5.5 c	27.5 ± 1.7 c	14.9 ± 1.4 a,b	20.3 ± 2.0 a,b,c	18.6 ± 1.6 a,b,c	15.7 ± 1.8 a,b	21.4 ± 2.0 b,c
Mitochondrion area/protoplast area, %								
Mestome sheath	0.5 ± 0.1 a	1.4 ± 0.4 a,b	3.4 ± 0.7 b	8.2 ± 0.8 c	10.6 ± 1.1 c	9.1 ± 0.8 c	2.2 ± 0.2 b	1.6 ± 0.1 b
Mesophyll	0.4 ± 0. 1 a	0.8 ± 0.1 b,c	1.6 ± 0.2 d,e	1.8 ± 0.2 e	1.2 ± 0.2 c,d	0.6 ± 0.1 a,b,c	1.0 ± 0.1 c,d	0.5 ± 0.1 a,b
Parenchymatous sheath	0.2 ± 0.0 a	1.0 ± 0.2 b,c,d	0.9 ± 0.1 b,c	0.5 ± 0.1 b	1.0 ± 0.1 c,d	0.7 ± 0.1 b	1.4 ± 0.2 d	0.8 ± 0.1 b,c
Mitochondrion #/protoplast area, $\mu m^{-2} \times 10^{-3}$								
Mestome sheath	47 ± 24 a	100 ± 25 b,c	164 ± 24 c,d	313 ± 23 e,f	389 ± 24 f	246 ± 24 d,e	53 ± 24 a,b	53 ± 24 a,b
Mesophyll	1.8 ± 0.2 a	2.9 ± 0.3 a,b	7.0 ± 0.7 c	6.8 ± 0.6 c	5.2 ± 0.8 b,c	2.4 ± 0.3 a	2.8 ± 0.3 a,b	2.2 ± 0.2 a
Parenchymatous sheath	1.2 ± 0.2 a	4.9 ± 0.8 b,c	5.6 ± 0.6 b,c	3.4 ± 0.3 c	6.0 ± 0.6 b	3.5 ± 0.4 c	4.3 ± 0.5 b,c	3.5 ± 0.5 c
Gold particles/mitochondrion area, μm^{-2}								
Mestome sheath	7.0 ± 3.5 a	47.3 ± 3.7 b,c	28.7 ± 3.5 b	37.4 ± 3.4 b,c	42.3 ± 3.5 bc	49.8 ± 3.5 c	23.8 ± 3.5 b	28.1 ± 3.5 b
Mesophyll	86.4 ± 5.8 a	53.1 ± 3.5 a	44.1 ± 2.1 a,b	46.1 ± 2.4 a	20.3 ± 1.7 b	2.2 ± 0.3 c	1.5 ± 0.3 c	2.0 ± 0.3 c
Parenchymatous sheath	53.9 ± 4.7 a	25.4 ± 2.4 a	16.2 ± 1.7 a	18.5 ± 1.3 a	4.0 ± 0.6 b	2.5 ± 0.4 b	1.3 ± 0.3 b	3.3 ± 0.7 b
Gold particles/protoplast area, μm^{-2}								
Mestome sheath	0.07 ± 0.28 a	0.84 ± 0.29 b,c	1.45 ± 0.28 c	2.92 ± 0.27 d	4.42 ± 0.28 d	4.39 ± 0.27 d	0.50 ± 0.27 b	0.44 ± 0.28 b
Mesophyll	0.32 ± 0.04 a,b	0.42 ± 0.06 a,b	0.76 ± 0.12 a,b	0.83 ± 0.09 a	0.29 ± 0.06 b	0.01 ± 0.00c	0.01 ± 0.00 c	0.01 ± 0.00 c
Parenchymatous sheath	0.13 ± 0.02a	0.19 ± 0.03 a	0.15 ± 0.02 a	0.10 ± 0.01 a	0.04 ± 0.01 b	0.02 ± 0.00 b	0.02 ± 0.00 b	0.02 ± 0.00 b

[a]Incomplete C_2 phenotype. [b]Complete C_2 phenotype, where all GDC is in the MS compartment.

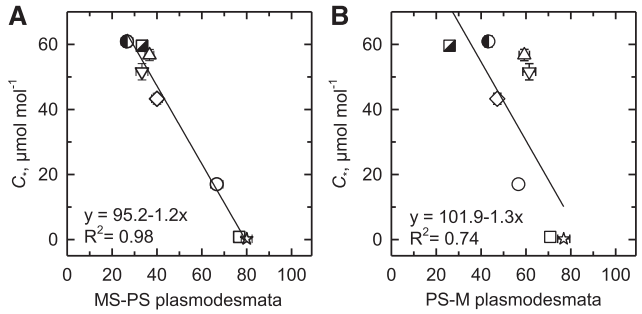

Figure 7. The relationship between C_* and PD frequencies in walls between leaf tissue types. A, The frequency of PD between MS and PS cells. B, The frequency of PD between PS and M cells. Mean ± SE; $n = 3$ plants per species; 10 images per plant. Significant linear regressions at $P \leq 0.05$ are shown. *N. alopecuroidea* (◑), *N. annularis* (▽), *N. lanigera* (◇), *N. minor* (○), *N. munroi* (□), *N. muelleri* (☆), *N. queenslandica* (△), and *T. mitchelliana* (◪). See Supplemental Table S3 for mean values and statistical tests.

(adjusted $R^2 = 0.99$, $P = 0.004$). This is consistent with significant regressions between individual variables and C_* in Figs. 3, 4, and 7.

Trait Reconstruction

The Neurachninae is nested within a C_3 clade in the Paniceae tribe (Grass Phylogeny Working Group II, 2012), and trait reconstructions support a hypothesis that the C_3 state represents the ancestral condition in the Neurachninae, with two origins of C_4 arising from an intermediate state (Fig. 9; Supplemental Table S7; Christin et al., 2012; Grass Phylogeny Working Group II, 2012). Ancestral state reconstruction of physiological (C_* or Γ), cellular (percent GDC in MS), and anatomical (MS L:W) traits using the Neurachninae phylogeny of Christin et al. (2012) consistently show intermediate trait values along the internal branches of the phylogeny, as indicated in Figure 9 by darker (for C_4) versus lighter (for C_3) shading on the branches (see also Supplemental Table S7). The 95% confidence interval (CI) for C_* and numerous other traits overlaps with the CI observed for C_3 species at nodes 1, 7, or 8 only, supporting a hypothesis that the ancestral state of the internal nodes 2–6 was C_2-like or proto-Kranz (Fig. 9; Supplemental Table S7). Although the trait reconstruction indicates the backbone of the *Neurachne* phylogeny corresponds to a C_2-like condition. Alternatively, the backbone of the tree could be predominantly C_3, with multiple origins of C_2 and C_4 species. Resolution of these alternative models may require discovery of additional populations and/or species of *Neurachne*, a possibility suggested by the relatively recent discovery of *N. annularis* by Macfarlane (2007).

DISCUSSION

In this work, we present a comprehensive analysis of changes in structure and enzyme distribution associated with the C_3 to C_4 transition in the grass subtribe Neurachninae. We demonstrate correlated shifts in multiple structural traits of leaves, and in the density

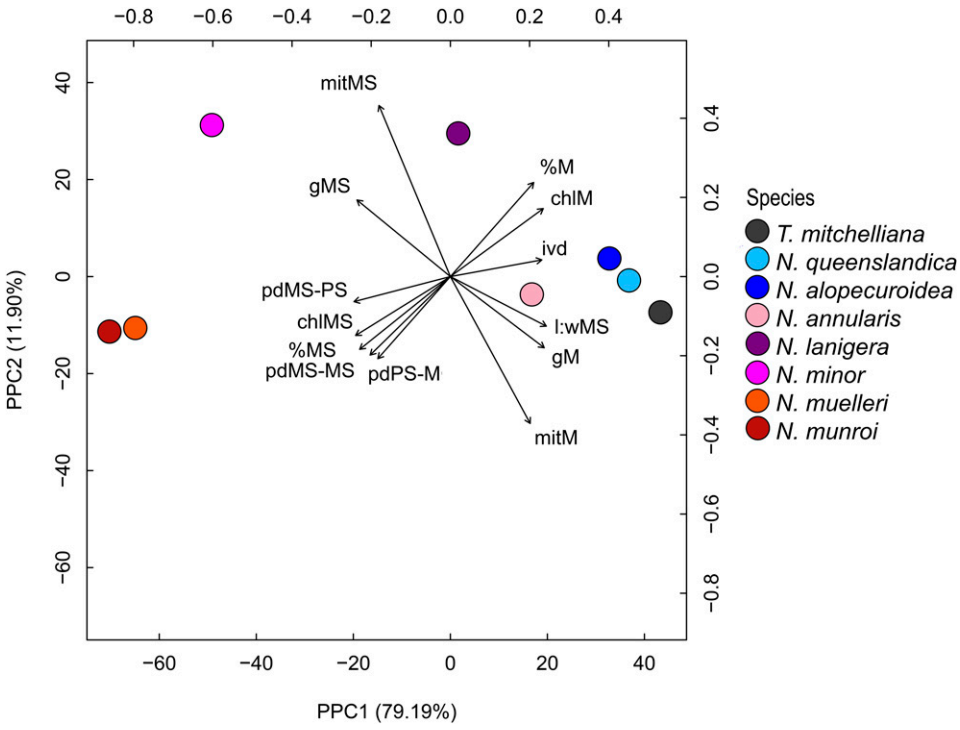

Figure 8. pPCA for eight species of Neurachnineae and correlation of 13 quantified variables with the first and second principal component. Data points indicate mean values for each species. Capital letters indicate cell or tissue type: M, PS, and MS. Small letters indicate measured variables as follows: chl, pecent chloroplast allocated to the specified tissue type; mit, percent mitochondria allocated to the specified tissue type; ivd, interveinal distance; g, GLDP density. See Supplemental Tables S1–S3 for mean values and allocation calculations.

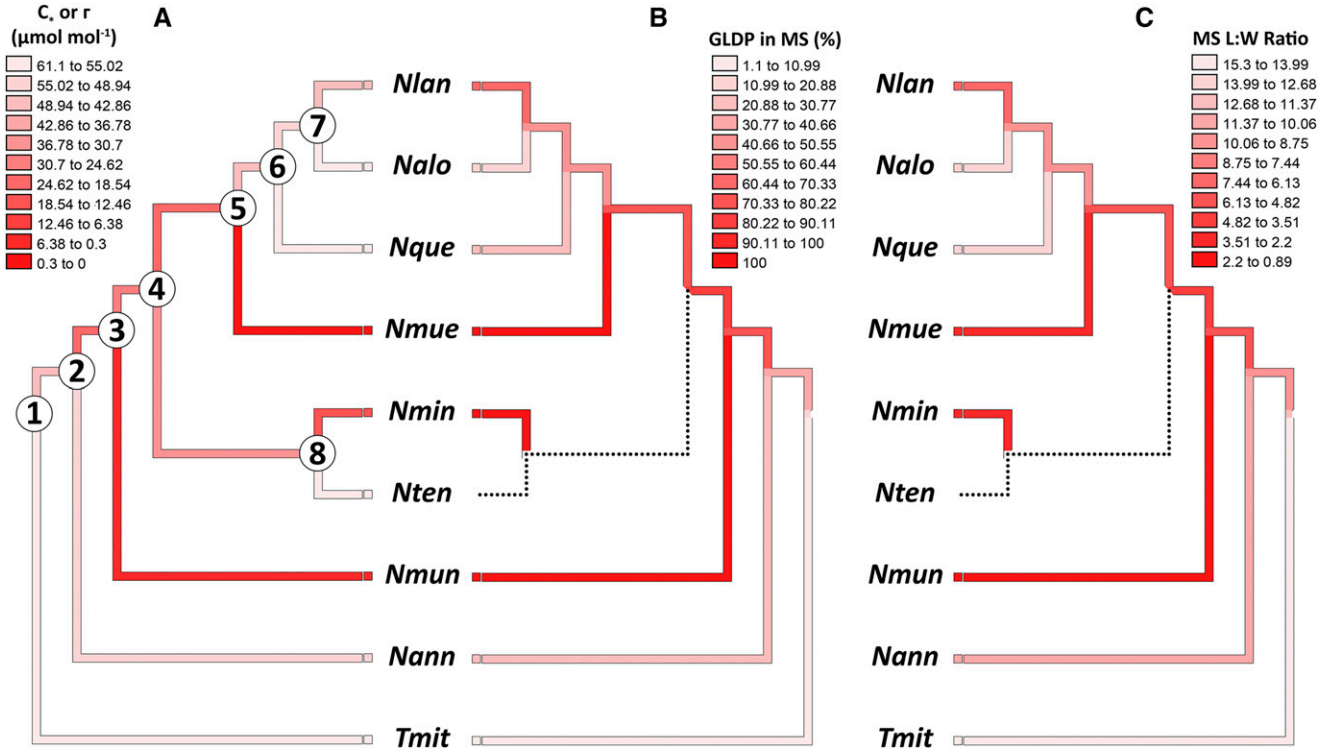

Figure 9. The molecular phylogeny of the Neurachninae (from Christin et al., 2012) with three traits mapped onto the tree. A, Values for C_*. B, % of GDC in the MS tissue. C, L:W of MS cells in paradermal section. No data were available for *N. tenuifolia*, as indicated by the dotted branch. Nlan, *N. lanigera*; Nalo, *N. alopecuroidea*; Nque, *N. queenslandica*; Nmue, *N. muelleri*; Nmin, *N. minor*; Nten, *N. tenuifolia*; Nmun, *N. munroi*; Nnann, *N. annularis*; Tmit, *T. mitchelliana*. Ninety-five percent confidence intervals for C_* and 12 other traits at ancestral nodes are presented in Supplemental Table S7.

and location of GLDP and Rubisco LSU in the observed C_3, C_2, and C_4 species of the Neurachninae. These variations are correlated with C_* and Γ, implying that simultaneous evolutionary modifications occurred to first assemble a C_2 pathway and then upregulate the C_4 pathway during the evolution of the two known C_4 clades in the Neurachninae. A key question is whether the phenotypes in the extant species represent the evolutionary phases that occurred in the transition from C_3 to C_4 photosynthesis in *Neurachne*, as opposed to being distinct nonintermediate states, for example, as may arise by reversion or hybridization events (Kadereit et al., 2017). In other clades of C_4 origin, phylogenetic data supports the hypothesis that intermediate phenotypes represent bona fide evolutionary states, as indicated by correspondence between phylogenetic and phenotypic gradients (McKown et al., 2005; Christin et al., 2011b; Yang and Berry, 2011; Sage et al., 2013; Fisher et al., 2015; Lundgren et al., 2016; Schüssler et al., 2017; Dunning et al., 2019). The Neurachninae phylogeny does not clearly follow these patterns, however. Hypotheses supported by the Neurachninae phylogeny of Christin et al. (2012; see also Fig. 9) include the following: (1) C_3 is the ancestral condition in the Neurachninae as indicated by the phylogenetic sister position of C_3 *Thyridolepis* and the nesting of the Neurachninae in a C_3 clade by the Grass Phylogeny Working Group (GPWGII, 2012). (2) In *Neurachne* itself, *N. annularis* branches at the base of the genus, allowing us to infer the proto-Kranz state described here is the ancestral condition within *Neurachne*. (3) *N. minor* branches in a sister position to the two C_4 species, supporting a hypothesis that it shares an intermediate common ancestor with the C_4 species. (4) A phylogenetic reconstruction within *Neurachne* indicates the ancestral state along the backbone of the genus tree is an intermediate condition that could have given rise to C_3 revertants, fully developed C_2 species, and multiple origins of C_4 species (Fig. 9).

The position of *N. lanigera* in the tree is intriguing because it is nested within a C_3 clade that is sister to the C_4 *N. muelleri*. This raises a number of possibilities. First, *N. lanigera*, *N. alopecuroidea*, and *N. queenslandica* may have been derived via reversion from an *N. muelleri*-like C_4 ancestor. This is unlikely because unequivocal evidence of reversion from a C_4 state has yet to be presented, and revertants may have poor fitness because they may not readily reacquire a functional C_3 pathway in the M tissue (Christin et al., 2010; Oakley et al., 2014; Bräutigam and Gowik, 2016). In addition, Christin et al. (2012) present evidence indicating *N. muelleri* obtained a C_4-adapted PEPC gene by lateral transfer from an ancestor of *N. munroi*. If *N. lanigera*, *N. alopecuroidea*, or *N. queenslandica* were revertants, they would be expected

to share this introgressed gene, which they do not (Christin et al., 2012). It is also possible that the partial C_2 physiology of *N. lanigera* is the result of $C_3 \times C_4$ hybridization. Evidence of $C_3 \times C_4$ hybridization in *Neurachne* was noted by Christin et al. (2012) through incongruence of chloroplast and nuclear genomes in polyploid *N. queenslandica*. The accession of *N. lanigera* used in this study is diploid (Christin et al., 2012), implying that it is not a hybrid. The available evidence supports a third interpretation, that *N. lanigera* ultimately arose de novo from an ancestral C_3 state. Resolution of this issue will require additional populations or species of *Neurachne* and/or detailed analysis of genomic data, which are underway. For now, the most parsimonious interpretation is that *N. lanigera* is derived from the C_3 condition by vertical selection, and thus may represent a genuine intermediate state in the evolution of full C_2 photosynthesis. If it is assumed the *N. annularis* and *N. minor* are also derived vertically from C_3 ancestors, and that C_* reflects the degree of intermediacy, then a hypothetical model of C_2 evolution can be generated for *Neurachne*.

The novel physiological and structural phenotypes shown here demonstrate the Neurachninae is more dynamic with respect to C_3–C_4 intermediacy than previously understood. Instead of containing just one C_3–C_4 intermediate species as described in Hattersley et al. (1986), the Neurachninae contains three intermediate species of differing character states. If the assumption that C_* reflects degrees of evolutionary intermediacy is valid, then the results are consistent with a progressive model of C_4 evolution as proposed for eudicot lineages such as *Flaveria* (Monson and Rawsthorne, 2000; Sage et al., 2013; Schulze et al., 2013; Bräutigam and Gowik, 2016). The structural and immunolocalization data provide some key details of how the C_2 pathway may have been assembled in *Neurachne*, and in the process highlight similarities with *Flaveria*, but also differences associated with the co-option of the MS versus BS tissue as the compartment of CO_2 concentration. To summarize, *N. annularis* has a higher organelle investment within the MS compared to the average of completely C_3 species, whereas *N. lanigera* has greater organelle investment that is intermediate between *N. annularis* and *N. minor*. *N. annularis* shows higher labeling of GLDP per MS protoplast, nearly double that of completely C_3 species, and approaching the high values observed in *N. lanigera* and *N minor*; however, *N. annularis* maintains a C_3-like pattern of GLDP expression in the M tissue. GLDP labeling in the M tissue of *N. lanigera* is half that of *N. annularis*, and is negligible in *N. minor*, typical of other well-developed C_2 species (Khoshravesh et al., 2016). *N. annularis* also exhibits initial characteristics of Kranz anatomy, as indicated by a 20% to 30% reduction in L:W of MS cells compared to the completely C_3 species. The L:W of the MS cells is even lower in *N. lanigera*, with values that are 50% of the completely C_3 species values, and in *N. minor* where L:W average 25% of the completely C_3 values. These changes in physiological and cellular characteristics are associated with lower C_* values: C_* in *N. annularis* is at the low end of the C_3 range, whereas C_* in *N. lanigera* falls between the C_3-like value of *N. annularis* and the completely C_2 value of *N. minor*. From these results, we conclude *N. annularis* is largely C_3 in function but shows evidence for an incipient C_2 cycle in the MS tissue, similar to what has been described in BS tissue of proto-Kranz species of *Flaveria*, *Heliotropium*, *Salsola*, and *Steinchisma* (Muhaidat et al., 2011; Sage et al., 2013; Khoshravesh et al., 2016, Schlüssler et al., 2017). *N. annularis* differs from proto-Kranz eudicots by not exhibiting a centripetal arrangement of mitochondria, but the thick suberized wall, coupled with the PS layer, indicates the accumulation of photorespiratory CO_2 released by MS mitochondria, thereby improving Rubisco efficiency. *N. lanigera* shows evidence for a stronger C_2 cycle, but this is not fully optimized for C_2 photosynthesis as it is in *N. minor*, largely due to the continued presence of GDC in the M cells. We conclude *N. lanigera* is an incomplete or partial C_2 species (C_2-like) that relies upon the MS mitochondria to metabolize some of the photorespiratory Gly from M tissue. In doing so, C_* is lowered to 44 μmol mol^{-1} at 35°C. The near complete loss of GLDP expression in the M tissue of *N. minor* results in the vast majority of photorespiratory Gly being metabolized in the MS tissue. Because of an abundance of mitochondria in the MS tissue, this species has sufficient capacity to metabolize all the photorespiratory Gly coming from the M tissue, and consequently, to reduce C_* to $<$20 μmol mol^{-1} as is often observed in completely C_2 species (Monson and Rawsthorne, 2000). The pronounced anatomical shifts in *N. minor* relative to C_3 species, including a lower MS cell L:W, greater MS volume, and higher PD frequency, demonstrate extensive cellular elaboration and developmental modification to support the C_2 pathway. *N. minor* can thus be considered to express a form of Kranz anatomy that is highly specialized for efficient C_2 function.

PD frequency through BS–M cell walls is known to be greater in C_4 than C_3 species (Hattersley et al., 1986; Danila et al., 2016, 2018). Data from this study likewise show more frequent PD through MS–PS cell walls, as well as through the PS–M and MS–MS cell walls of the C_4 Neurachninae. Moreover, results demonstrated there is a significant relationship between C_* and PD frequency through the MS–PS cell walls, and C_* and PD frequency through PS–M walls. Assuming C_* reflects the degree of C_3–C_4 intermediacy, these results are consistent with a model whereby the increase in PD is progressive across the C_3–C_4 transition in the Neurachninae. Because enhancement of PD frequency also occurs in proportion to greater organelle and GLDP labeling in the MS tissue, we conclude that a greater flux of photorespiratory metabolites is linked to formation of more PD. PD enhancement in the Neurachninae could be due to increased levels of *GOLDEN2-LIKE* (*GLK*) transcription factors, which have been hypothesized to promote activation of BS cells during C_4 evolution (Waters et al., 2009). In rice (*Oryza sativa*), constitutive expression of *GLK* genes resulted in greater chloroplast and

mitochondrial volume in BS and MS cells that corresponded with more Rubisco and GLDP content as well as higher PD frequency between M and BS cells (Wang et al., 2017), similar to what is observed in *N. annularis* and *N. lanigera*.

Declines in M cell number and size contribute to reductions in IVD in C_4 relative to C_3 leaves and are considered essential for optimal C_4 function because fewer M cells reduce the mean diffusion distance for C_4 cycle metabolites (Hattersley, 1984; Dengler and Nelson, 1999; Ogle, 2003; Griffiths et al., 2013). The reduction in IVD in Neurachninae species occurs in proportion to a decline in C_*, and is due to progressively fewer M cells between veins. In the C_4 *N. munroi* and *N. muelleri*, these changes converge upon approximately two M cells between the veins, a commonly observed number in most C_4 lineages (Hattersley and Watson, 1975; Dengler and Nelson, 1999; Christin et al., 2013). Notably, reductions in IVD are apparent in *N. annularis* and *N. lanigera* compared to the completely C_3 *N. alopecuroidea* and *T. mitchelliana*. In *N. minor*, two M cells are already apparent between veins and IVD approaches C_4 values, indicating that the rapid flux of photorespiratory metabolites between M and MS tissues in this C_2 species requires short diffusion distances that are similar to C_4 values. If so, meeting the rapid transport imperative in C_2 photosynthesis establishes the low transport distance required for efficient C_4 function.

Enhanced BS cell size is commonly thought to be essential for C_4 function by allowing for greater organelle volume, and creating a large vacuole in species lacking suberized lamellae (Dengler and Nelson, 1999; Christin et al., 2013). Large vacuoles can serve as a resistive barrier that facilitates CO_2 trapping in sheath tissues (von Caemmerer and Furbank, 2003). Because it is uncertain where along the C_3–C_4 transition that the size of the Kranz sheath cell increases, we examined changes in MS cell morphology in three dimensions among the various photosynthetic types. In contrast to the common view, we observed no correlation between C_* and MS volume. MS cells of C_4 *Neurachne* species are not larger (that is, more voluminous) than their C_3 counterparts, although they are wider and shorter. The MS cell dimensions changed such that the L:W was ~80% lower in the C_4 than in the C_3 species. Danila et al. (2018) also noted C_3 and C_4 grasses have similar BS cell volume. Based on results from the Neurachninae and Danila et al. (2018), we conclude that Kranz anatomy in grasses does not consist of larger BS or MS cells, but only an increased width of BS or MS cells. As indicated by the proportional decline in C_* and the L:W of MS cells, the evolutionary reorientation of the MS cells may have occurred progressively in *Neurachne*, with *N. annularis* representing an early stage in this process. The change in MS tissue shape arises from a reorientation in the polarity of cell expansion from a pattern emphasizing proximo-distal (lengthwise, or base to tip in a grass leaf) to medio-lateral (widthwise) expansion, with an increase in cell division along the proximo-distal axis. In doing so, the MS tissue volume (rather than cell volume) increases, creating additional space for organelles and possibly increasing the diffusive distance for CO_2 efflux. The increase in MS cell division along the proximo-distal leaf axis is in contrast to declines in M cell division along the medio-lateral leaf axis, highlighting the contrasting shifts in tissue development from C_3 to C_2 to C_4 phenotypes.

A Model of C_2 Evolution in the Neurachninae

Understanding of the evolutionary origin of C_4 photosynthesis is largely based on eudicot systems, notably *Flaveria* (Monson and Rawsthorne, 2000; Sage et al., 2013; Schulze et al., 2013; Covshoff et al., 2014). Evolution in monocots is less understood due to the low number of C_3–C_4 intermediates in grasses and sedges that have been identified and studied (Sage et al., 2011a; Lundgren and Christin, 2017). For monocots, this deficiency constrains development of evolutionary landscape models of C_4 origin. Williams et al. (2013) used a Bayesian approach to fill in gaps in the evolutionary sequence of monocots and coupled this to a Markov model to compare evolutionary landscapes in eudicots and monocots. Only two C_3–C_4 intermediate monocots (*N. minor* and *Steinchisma hians*) were available to parameterize the monocot responses and both exhibit well-developed C_2 photosynthesis (Williams et al., 2013; Khoshravesh et al., 2016). The model predicted significant divergence in the paths to C_4 photosynthesis, with monocots delaying reallocation of GDC to the sheath cells relative to eudicots. Monocots were also predicted to delay chloroplast accumulation and enhancement of sheath size in comparison with eudicots, while accelerating reductions in vein spacing. Our results do not support these interpretations of Williams et al. (2013). The *Neurachne* data, along with recent results from *Flaveria* (Sage et al., 2013; Schulze et al., 2013), *Heliotropium* (Muhaidat et al., 2011), and *Steinchisma* (Brown et al., 1983; Khoshravesh et al., 2016) show similar patterns in organelle enhancement and GDC reallocation in grasses and eudicots. Instead of multiple distinct evolutionary pathways between monocots and eudicots, as concluded by Williams et al. (2013), the pattern we interpret is one of similarities between monocots and eudicots in terms of first acquiring the C_2 pathway via organelle and GDC enrichment in the sheath cells, concurrent with reductions in IVD. This new information, along with recent data from *Alloteropsis semialata* intermediates (Lundgren et al., 2019), will be valuable in updating the Williams et al. (2013) model. Whereas significant differences in the general pattern of C_2 evolution are not obvious, subtle differences are observed between *Flaveria* and *Neurachne*, which are two lineages with enough variation between intermediates to evaluate potential patterns of evolutionary change. The nature of the ancestral sheath tissue likely accounts for these variations.

From studies of both eudicots and *Neurachne*, the initial phase of C_2 evolution appears to be the accumulation of organelles in the sheath tissue (BS in *Flaveria*, *Heliotropium*, and *Euphorbia*, MS in *Neurachne*), to strengthen, or "activate," the photosynthetic potential of the sheath tissue (Muhaidat et al., 2011; Sage et al., 2011b, 2013; Schulze et al., 2013). In C_3 *Flaveria*, *Euphorbia*, and *Heliotropium*, this activation occurs in tandem with increased BS width. In C_3 *Flaveria cronquistii*, chloroplasts and mitochondria line the walls along the intercellular air spaces (IAS), allowing the BS cells to conduct diffusion-based C_3 photosynthesis as occurs in the M cells (Sage et al., 2013). CO_2 rapidly diffuses into the peripheral BS chloroplasts from the IAS while adjacent mitochondria quickly recycle photorespiratory metabolites (Bauwe et al., 2010). The shift to the proto-Kranz phase is observed in *Flaveria pringlei* and *Flaveria robusta*, which are branch sisters to *F. cronquistii* in the *Flaveria* phylogeny. In these two species, the mitochondria are repositioned along the centripetal wall of the BS cells, opposite most chloroplasts. Similar relocation of mitochondria occurs in the BS of proto-Kranz *Heliotropium*, *Salsola*, and *Steinchisma* species (Sage et al., 2014). This relocation leads Gly produced from glycolate made in the peripheral chloroplasts to be metabolized by centripetal mitochondria, with the result that photorespiratory CO_2 accumulates in the inner region, enhancing Rubisco efficiency in nearby chloroplasts. This arrangement is proposed to establish a single-cell Gly shuttle that can scavenge some photorespiratory CO_2 with slight benefits to the plant (Sage et al., 2013, 2014).

In *Neurachne* and *Thyridolepis*, MS cells have suberized outer walls and are surrounded by tightly packed PS cells, both of which can enhance resistance to diffusive efflux of CO_2 generated by decarboxylation of Gly or C_4 acids (Hattersley et al., 1986; von Caemmerer and Furbank, 2003; Alonso-Cantabrana et al., 2018). In the MS of C_3 species, however, suberized walls and the PS sheath would reduce diffusive CO_2 influx and thus starve chloroplasts of CO_2. A boost in chloroplast numbers in the MS of C_3 species would therefore be of little value unless CO_2 were imported from another source, such as photorespiratory Gly. Because *N. annularis* grows in warm-temperate, semiarid landscapes of western Australia with hot summers (Macfarlane, 2007), high rates of photorespiration would produce an abundance of Gly that could potentially deliver CO_2 to the MS cells. If elevated GDC activity reduces Gly concentration in the MS, a Gly diffusion gradient between M and MS cells would be established, thereby drawing in additional Gly. We hypothesize that the boost in organelles in the MS of *N. annularis* creates a sink for photorespiratory Gly and can thus increase photosynthetic potential in the MS cells in a manner that slightly enhances leaf photosynthetic efficiency. Because this enhancement results from the operation of a weak photorespiratory Gly shuttle, we propose *N. annularis* fits the criteria of the proto-Kranz species, even though there is no mitochondrial relocation within the MS cell as observed in eudicots. We hypothesize the suberized walls and PS in *N. annularis* slow CO_2 efflux, thereby eliminating the need to reposition mitochondria, whereas in *Flaveria* and other eudicots, trapping of photorespired CO_2 requires a wide vacuole between centripetal mitochondria and the outer periphery of the BS cells to form the barrier to CO_2 efflux.

As indicated by the phenotypes of the C_2-like species *N. lanigera* and *Flaveria angustifolia*, once numerous organelles are in place in the sheath tissue and a limited photorespiratory Gly shuttle is functioning, step-wise progression to an optimized C_2 pathway is envisioned where parallel changes occur in (1) increased organelle number in the sheath tissue, (2) greater GDC content in the sheath tissue, (3) reduction of GDC in M cells, (4) increasing PD connections between sheath and M tissue, and (5) increasing Kranz-like anatomy via fewer M cells between veins and declining MS L:W, resulting in increased proportion of BS or MS cell area in cross section (Sage et al., 2013). Because the establishment of a Gly sink in the sheath tissue is beneficial during high photorespiratory episodes, it may stabilize the proto-Kranz character state in hot climates and by doing so become a foundation that enables subsequent evolution that strengthens the photorespiratory Gly shuttle (Sage et al., 2012; Mallmann et al., 2014; Bräutigam and Gowik 2016). As has been proposed for later stages in C_4 evolution (from the C_2 to C_4 condition), this "facilitation" cascade could establish an evolutionary trajectory that resembles a Mount Fuji-type of fitness landscape (Heckmann et al., 2013).

CONCLUSION

The information presented here from the Neurachninae indicates how the structural requirements for C_4 photosynthesis are largely met by the evolution of the C_2 pathway, where MS tissue width, PD frequency, and IVD in *N. minor* equals or approaches C_4 values. This illustrates how the evolution of C_2 photosynthesis could establish the foundation of structure and metabolite transport upon which a C_4 metabolic cycle may be assembled. We also provide evidence that is consistent with a model whereby the assembly of the C_2 pathway occurs gradually, beginning with modifications in MS cell division and expansion, reduced M cell division, and greater organelle allocation to the MS cells. Assuming C_* reflects the degree of evolutionary intermediacy, the results support a hypothesis that organelle enrichment initiates a progressive reallocation of GDC from M to MS tissue, with loss of GDC expression in M cells occurring after mitochondrial enhancement increases GDC capacity in the MS tissue. Pre-existing anatomy in *Neurachne* likely eliminates the need for the repositioning of organelles observed in eudicots, because the PS and thick MS wall enable CO_2 trapping without a need for a large vacuole acting as a diffusive barrier. In light of these

results, the Neurachninae, along with numerous eudicot groups such as *Flaveria*, indicates how evolutionary processes reconfigured the variable anatomy, biochemistry, and physiology of C_3 ancestors into a common, complex trait that can address challenges imposed by global environmental change.

MATERIALS AND METHODS

Plant Material

Seeds or rhizomes of *Thyridolepis mitchelliana*, *Neurachne alopecuroidea*, *Neurachne annularis*, *Neurachne lanigera*, *Neurachne minor*, *Neurachne queenslandica*, *Neurachne tenuifolia*, *Neurachne munroi*, and *Neurachne muelleri* were collected in their natural habitat (Supplemental Table S8) and used to generate plants that were grown in naturally illuminated glasshouses at the Plant Growth Facility, University of Western Australia, Perth, Western Australia (latitude 33°59′ south). *N. muelleri* was classified by Blake (1972) as *Paraneurachne muelleri* but was previously known as *N. muelleri* (Hackel, 1895; Lazarides, 1970). As a recent molecular study showed the species branches within the Neurachne phylogeny (Christin et al., 2012), the original name is used here. *T. mitchelliana*, *N. alopecuroidea*, *N. annularis*, and *N. tenuifolia* were grown at mean temperatures of 22°C/18°C (day/night), whereas *N. lanigera*, *N. minor*, *N. munroi*, and *N. muelleri* were grown at mean temperatures of 30°C/25°C (day/night). *N. queenslandica* was grown at day/night temperatures of 28°C/18°C in a separate, sealed greenhouse, as it is not native to Western Australia and thus by regulatory statute required complete isolation from the outside environment. Plants were grown in a mixture of a commercial potting mix and soil collected from west-central Australia, and fertilized with slow release fertilizer for Australian native plants (Osmocote Plus Trace elements: Native Gardens, Scotts Australia). Growth photon flux density routinely reached 1,600 μmol m^{-2} s^{-1}. Recently fully expanded leaves of mature plants were used for all measurements. All species were examined for gas exchange, microscopic imaging, and immunolocalization analysis except for *N. tenuifolia*, which died after preliminary sampling and was unavailable for immunolocalization and gas exchange analyses.

Whole-Leaf Gas Exchange

Leaf gas exchange measurements were performed on healthy, attached leaves using a model no. LI-6400XT gas exchange system (LICOR Biosciences). Responses of net CO_2 assimilation rate (A) to intercellular CO_2 concentration (C_i) were measured at a leaf temperature of 32°C and a light intensity of 1,500 μmol m^{-2} s^{-1}. After a leaf was acclimated to these conditions inside the LI-6400XT leaf chamber, the A/C_i curves were measured with a sequence of reference CO_2 concentrations of 400, 300, 200, 150, 100, 75, 50, 400, 400, 600, 800, 1,000, 1250, 1,500, and 2,000 μmol mol^{-1}. Data were recorded in quick sequential order, with an equilibration time of between 90 and 180 s at each CO_2 concentration. The CO_2 compensation point in the absence of day respiration (C_*) was measured using the common-intercept method at 35°C (Brooks and Farquhar, 1985). For the C_* measurements, leaves were acclimated to a leaf temperature of 35°C, a light intensity of 1,000 μmol m^{-2} s^{-1}, and a reference CO_2 concentration of 400 μmol mol^{-1} until A reached steady state. CO_2 responses were then measured at CO_2 concentrations of 400, 120, 110, 100, 90, 80, 70, and 60 μmol mol^{-1} at five different light intensities of 1,000, 400, 300, 200, and 150 μmol m^{-2} s^{-1}. At each light intensity, leaves were given an additional 10 min to acclimate before proceeding with the next CO_2 step change. Typically, lower light intensity reduces the slope of the A versus C_i plot at low C_i, creating a distinct series of linear responses that can be used to estimate C_* by plotting the regression slope of these responses versus their corresponding y-intercept (Walker and Ort, 2015). C_* is then estimated as the slope of this relationship, assuming that M conductance is constant (Supplemental Fig. S1; Walker and Ort, 2015; Walker et al., 2016). Outlier points at high light were excluded from the regression analysis if they resulted from shifts in the A/C_i response to lower C_i, as can occur in C_2 species at >800 μmol photons m^{-2} s^{-1} (Sage et al., 2013). In C_4 plants, the common intercept method does not work for C_* as Γ varies little with declining photosynthetic photon flux density (Table 1); hence, only Γ values were determined in C_4 plants at saturating light.

Leaf Anatomy, Ultrastructure, and Immunolocalization

The internal anatomy of leaves was assessed on sections sampled from the middle of the most recent, fully expanded leaves (three plants per species; one leaf per plant; 10 images per leaf). Plants were sampled between 9 AM and 12 AM. The youngest cohort of fully expanded leaves was sampled in full sun for all procedures. Samples were fixed in 0.5% (v/v) glutaraldehyde, 4% (w/v) paraformaldehyde in sodium cacodylate buffer for light and transmission electron microscopy (TEM), and embedded in Spurr's resin and London Resin White as described by Khoshravesh et al. (2017). Immunocytochemical detection of GLDP and Rubisco LSU followed Khoshravesh et al. (2016, 2017) with the same antibodies used for the immunoblots (Supplemental Fig. S4; see Supplemental Table S9 for more details). Light microscope images were obtained with an Axioplan (Zeiss) equipped with an image analysis system (model no. DP71, Olympus; Empix Imaging). A Philips 201 TEM equipped with an Advantage HR camera system (Advanced Microscopy Techniques) was used to capture leaf ultrastructure and immunolabeling results. To quantify all M, PS, and MS cellular features, and immunodetection events (gold particles) of GLDP and Rubisco LSU, TEM images were analyzed using a Cintiq graphics tablet (Wacom Technology) and ImageJ software (Schneider et al., 2012) as described in Sage et al. (2013) and Stata et al. (2014). To quantify protoplast area, we subtracted the cross-sectional area of the cell covered by cell walls from the cell area values. IVD was measured as the distance between PS tissue of minor veins, because the PS tissue is part of the vascular tissue complex. MS cell volume was estimated as the length along the proximo-distal axis parallel to the vein (in paradermal sections) times the area of the MS cell in planar cross section. Allocation coefficients representing the fraction of organelles and GLDP in specific tissues were calculated as: % organelle allocation = (planar area of an organelle within a tissue cross section divided by the sum of organelle area in all of the MS, M, and PS tissue within a sample image) × 100%; and percent GLDP allocation = (the number of immunogold particles within a tissue cross section divided by the total number of immunogold particles in the MS, M, and PS tissue within a sample image) × 100% (Wang et al., 2017). IAS were not included in tissue measurements. PD frequency was quantified as described by Wang et al. (2017); the presence and absence of PD in the walls between M, MS, and PS cells in planar cross sections of TEM images were recorded as absence = 0, presence = 1. Relative frequency of PD was then quantified as the number of cells that had PD connections with the adjacent cell, divided by the total number of observed cells for that cell-type, multiplied by 100%.

Data Analysis

For analysis of light microscopy and TEM images, samples were collected from one leaf of each of three distinct plants. Ten images from each leaf were analyzed with the values averaged to provide a mean for the plant. These individual plant values were the unit of replication for statistical analysis. For leaf gas exchange, three to eight measurements were conducted on two to seven plants per species, with each leaf serving as the unit of replication. Results were analyzed with the software SigmaPlot v12.5 (Systat Software) or SPSS v20.0. (IBM) using one-way ANOVA followed by a Tukey's test of variance (for normally distributed data) or a Games–Howell test (when the variances were not equal) to evaluate statistical grouping of the species means, unless otherwise indicated.

To analyze whether the anatomical variables and GLDP labeling predict C_* values in the Neurachninae, linear regression analysis was performed. Predictors were selected based on their correlation (Pearson correlation coefficient [r] $\geq |0.65|$) with C_*. To correct for phylogenetic signal, phylogenetic independent contrast on the mean value of selected traits was performed using the R package "ape" (Paradis et al., 2004), with evolutionary model = Brownian Motion. The list of predictors was then finalized by selecting traits exhibiting Pearson correlations coefficient (r) $\geq |0.65|$ with C_* in the contrasting analysis. To eliminate collinearity between selected variables, a phylogenetic pPCA was performed using the phylo.pca function from the R package phytools v0.6-44 (Revell 2009, 2012). Then a linear regression (principal component regression) was performed using pPCs with eigenvalues > 0.1 as the predictors.

To evaluate possible ancestral character states, C_*, percent GLDP in the MS, L:W of MS cell, plus other structural traits were mapped onto the Neurachninae phylogeny of Christin et al. (2012) using the program Mesquite (Maddison and Maddison, 2018) and maximum parsimony (Fig. 9). The 95% confidence intervals for physiological (C_* or for C_4 species, Γ), cellular, and anatomical traits were reconstructed using a maximum likelihood approach and Brownian

Motion evolutionary models using R package "ape" (Paradis et al., 2004) and the Neurachninae phylogeny (Christin et al., 2012; Supplemental Table S7).

Supplemental Data

The following supplemental materials are available.

Supplemental Appendix 1. Supplemental Tables S1-S9.

Supplemental Table S1. Characteristics of cells and tissues from Neurachninae leaves.

Supplemental Table S2. The allocation of organelles and GLDP in photosynthetic tissues of eight Neurachninae species.

Supplemental Table S3. Peroxisome parameters and PD frequency in eight Neurachninae species.

Supplemental Table S4. Pearson correlations coefficients between measured parameters in this study.

Supplemental Table S5. Summary of pPCA.

Supplemental Table S6. Pearson correlations coefficients between traits and phylogenetic principal components.

Supplemental Table S7. Means and 95% confidence interval for reconstructed trait values at the phylogenetic nodes in Figure 9.

Supplemental Table S8. Species examined, with voucher information and source location.

Supplemental Table S9. Details of immunolocalization methods.

Supplemental Appendix 2. Supplemental Figures S1–S9.

Supplemental Figure S1. The relationship between the initial slope of the *A*/*Ci* response and its extrapolated *y*-intercept for five species of *Neurachne*.

Supplemental Figure S2. Light micrographs of leaf cross sections from nine Neurachninae species.

Supplemental Figure S3. TEM images of MS cells in *N. queenslandica*, *N. tenuifolia*, and *T. mitchelliana*.

Supplemental Figure S4. Immunoblot and transcript analyses of *Neurachne* GLDP and the Rubisco LSU.

Supplemental Figure S5. TEM images of GLDP immunolocalization in M cells of six *Neurachne* species.

Supplemental Figure S6. Immunolocalization of Rubisco LSU in C_3 Neurachninae species.

Supplemental Figure S7. Immunolocalization of Rubisco LSU in *N. annularis*, *N. lanigera*, and *N. minor*.

Supplemental Figure S8. Immunolocalization of Rubisco LSU in C_4 *Neurachne species*.

Supplemental Figure S9. Phylogenetic independent contrast plots of pair comparisons between 13 anatomical traits selected for pPCA and C_*.

Received July 30, 2019; accepted October 2, 2019; published October 14, 2019.

LITERATURE CITED

Aliscioni SS, Giussani LM, Zuloaga FO, Kellogg EA (2003) A molecular phylogeny of *Panicum* (Poaceae: Paniceae): Tests of monophyly and phylogenetic placement within the Panicoideae. Am J Bot **90:** 796–821

Alonso-Cantabrana H, Cousins AB, Danila F, Ryan T, Sharwood RE, von Caemmerer S, Furbank RT (2018) Diffusion of CO_2 across the mesophyll-bundle sheath cell interface in a C_4 plant with genetically reduced PEP carboxylase activity. Plant Physiol **178:** 72–81

Bauwe H (2011) Photorespiration: The bridge to C_4 photosynthesis. In AS Raghavendra, and RF Sage, eds, C_4 Photosynthesis and Related CO_2 Concentrating Mechanisms. Springer, The Netherlands, pp 81–108

Bauwe H, Hagemann M, Fernie AR (2010) Photorespiration: Players, partners and origin. Trends Plant Sci **15:** 330–336

Blake ST (1972) *Neurachne* and its allies (Gramineae). Contributions from the Queensland Herbarium **13:** 1–53

Bräutigam A, Gowik U (2016) Photorespiration connects C_3 and C_4 photosynthesis. J Exp Bot **67:** 2953–2962

Brooks A, Farquhar GD (1985) Effect of temperature on the CO_2/O_2 specificity of ribulose-1,5-bisphosphate carboxylase/oxygenase and the rate of respiration in the light. Estimates from gas-exchange measurements on spinach. Planta **165:** 397–406

Brown RH, Bouton JH, Rigsby L, Rigler M; Ultrastructural Characteristics of Panicum Species in the Laxa Group (1983) Photosynthesis of grass species differing in carbon dioxide fixation pathways: VIII. Ultrastructural characteristics of *Panicum* species in the *laxa* group. Plant Physiol **71:** 425–431

Brown RH, Hattersley PW (1989) Leaf anatomy of C_3-C_4 species as related to evolution of c_4 photosynthesis. Plant Physiol **91:** 1543–1550

Busch FA, Sage TL, Cousins AB, Sage RF (2013) C_3 plants enhance rates of photosynthesis by reassimilating photorespired and respired CO_2. Plant Cell Environ **36:** 200–212

Christin P-A, Freckleton RP, Osborne CP (2010) Can phylogenetics identify C_4 origins and reversals? Trends Ecol Evol **25:** 403–409

Christin P-A, Osborne CP, Chatelet DS, Columbus JT, Besnard G, Hodkinson TR, Garrison LM, Vorontsova MS, Edwards EJ (2013) Anatomical enablers and the evolution of C_4 photosynthesis in grasses. Proc Natl Acad Sci USA **110:** 1381–1386

Christin PA, Osborne CP, Sage RF, Arakaki M, Edwards EJ (2011a) C_4 eudicots are not younger than C_4 monocots. J Exp Bot **62:** 3171–3181

Christin PA, Sage TL, Edwards EJ, Ogburn RM, Khoshravesh R, Sage RF (2011b) Complex evolutionary transitions and the significance of C_3-C_4 intermediate forms of photosynthesis in *Molluginaceae*. Evolution **65:** 643–660

Christin PA, Wallace MJ, Clayton H, Edwards EJ, Furbank RT, Hattersley PW, Sage RF, Macfarlane TD, Ludwig M (2012) Multiple photosynthetic transitions, polyploidy, and lateral gene transfer in the grass subtribe *Neurachninae*. J Exp Bot **63:** 6297–6308

Covshoff S, Burgess SJ, Kneřová J, Kümpers BMC (2014) Getting the most out of natural variation in C_4 photosynthesis. Photosynth Res **119:** 157–167

Danila FR, Quick WP, White RG, Furbank RT, von Caemmerer S (2016) The metabolite pathway between bundle sheath and mesophyll: Quantification of plasmodesmata in leaves of C_3 and C_4 monocots. Plant Cell **28:** 1461–1471

Danila FR, Quick WP, White RG, Kelly S, von Caemmerer S, Furbank RT (2018) Multiple mechanisms for enhanced plasmodesmata density in disparate subtypes of C_4 grasses. J Exp Bot **69:** 1135–1145

Dengler NG, Nelson T (1999) Leaf structure and development in C_4 plants. In RF Sage, and RK Monson, eds, C_4 Plant Biology. Academic Press, San Diego, pp 133–172

Downton WJ (1971) Adaptive and evolutionary aspects of C_4 photosynthesis. In MD Hatch, CB Osmond, and RO Slatyer, eds, Photosynthesis and Photorespiration. Wiley Interscience, New York, pp 3–32

Dunning LT, Moreno-Villena JJ, Lundgren MR, Dionora J, Salazar P, Adams C, Nyirenda F, Olofsson JK, Mapaura A, Grundy IM, et al (2019) Key changes in gene expression identified for different stages of C4 evolution in *Alloteropsis semialata*. J Exp Bot **70:** 3255–3268

Edwards GE, Voznesenskaya EV (2011) C_4 photosynthesis: Kranz forms and single-cell C4 in terrestrial plants. In AS Raghavendra, and RF Sage, eds, C_4 Photosynthesis and Related CO_2 Concentrating Mechanisms, Vol **Vol 32**. Springer, Dordrecht, pp 29–61

Fisher AE, McDade LA, Kiel CA, Khoshravesh R, Johnson MA, Stata M, Sage TL, Sage RF (2015) History of *Blepharis* (Acanthaceae) and the origin of C_4 photosynthesis in section *Acanthodium*. Int J Plant Sci **176:** 770–790

Gowik U, Westhoff P (2011) The path from C_3 to C_4 photosynthesis. Plant Physiol **155:** 56–63

Grass Phylogeny Working Group II (2012) New grass phylogeny resolves deep evolutionary relationships and discovers C_4 origins. New Phytol **193:** 304–312

Griffiths H, Weller G, Toy LFM, Dennis RJ (2013) You're so vein: Bundle sheath physiology, phylogeny and evolution in C_3 and C_4 plants. Plant Cell Environ **36:** 249–261

Hackel E (1895) Neurachninae muelleri n. sp. Österr Bot Zeitschr **45:** 329

Hattersley PW (1984) Characterization of C_4 leaf anatomy in grasses (poaceae). Mesophyll: Bundle sheath area ratios. Ann Bot **53:** 163–179

Hattersley PW, Roksandic Z (1983) Delta ^{13}C values of C_3 and C_4 species of Australian *Neurachne* and its allies (Poaceae). Aust J Bot **31:** 317–321

Hattersley PW, Stone NE (1986) Photosynthetic enzyme activities in the C_3-C_4 intermediate *Neurachne minor* Blake, S. T. (Poaceae). Aust J Plant Physiol **13:** 399–408

Hattersley PW, Watson L (1975) Anatomical parameters for predicting photosynthetic pathways of grass leaves: The 'maximum lateral cell count' and the 'maximum cells distant count'. Phytomorphology **25:** 325–333

Hattersley PW, Watson L, Johnston CR (1982) Remarkable leaf anatomical variations in *Neurachne* and its allies (Poaceae) in relation to C_3 and C_4 photosynthesis. Bot J Linn Soc **84:** 265–272

Hattersley PW, Wong S-C, Perry S, Roksandic Z (1986) Comparative ultrastructure and gas exchange characteristics of the C_3–C_4 intermediate *Neurachne minor* S. T. Blake (Poaceae). Plant Cell Environ **9:** 217–233

Heckmann D, Schulze S, Denton A, Gowik U, Westhoff P, Weber AP, Lercher MJ (2013) Predicting C_4 photosynthesis evolution: Modular, individually adaptive steps on a Mount Fuji fitness landscape. Cell **153:** 1579–1588

Kadereit G, Ackerly D, Pirie MD (2012) A broader model for C_4 photosynthesis evolution in plants inferred from the goosefoot family (Chenopodiaceae s.s.). Proc Biol Sci **279:** 3304–3311

Kadereit G, Bohley K, Lauterbach M, Tefarikis DT, Kadereit JW (2017) C_3-C_4 intermediates may be of hybrid origin—a reminder. New Phytol **215:** 70–76

Kadereit G, Lauterbach M, Pirie MD, Arafeh R, Freitag H (2014) When do different C_4 leaf anatomies indicate independent C_4 origins? Parallel evolution of C_4 leaf types in Camphorosmeae (Chenopodiaceae). J Exp Bot **65:** 3499–3511

Keerberg O, Pärnik T, Ivanova H, Bassüner B, Bauwe H (2014) C_2 photosynthesis generates about 3-fold elevated leaf CO_2 levels in the C_3-C_4 intermediate species *Flaveria pubescens*. J Exp Bot **65:** 3649–3656

Khoshravesh R, Lundsgaard-Nielsen V, Sultmanis S, Sage TL (2017) Light microscopy, transmission electron microscopy, and immunohistochemistry protocols for studying photorespiration. In AR Fernie, H Bauwe, and APM Weber, eds, Photorespiration: Methods and Protocols. Springer, New York, pp 243–270

Khoshravesh R, Stinson CR, Stata M, Busch FA, Sage RF, Ludwig M, Sage TL (2016) C_3-C_4 intermediacy in grasses: Organelle enrichment and distribution, glycine decarboxylase expression, and the rise of C_2 photosynthesis. J Exp Bot **67:** 3065–3078

Lazarides M (1970) The Grasses of Central Australia. Australian National University Press, Canberra, ACT, Australia

Leegood RC (2008) Roles of the bundle sheath cells in leaves of C3 plants. J Exp Bot **59:** 1663–1673

Lundgren MR, Christin P-A (2017) Despite phylogenetic effects, C_3-C_4 lineages bridge the ecological gap to C_4 photosynthesis. J Exp Bot **68:** 241–254

Lundgren MR, Christin P-A, Escobar EG, Ripley BS, Besnard G, Long CM, Hattersley PW, Ellis RP, Leegood RC, Osborne CP (2016) Evolutionary implications of C_3-C_4 intermediates in the grass *Alloteropsis semialata*. Plant Cell Environ **39:** 1874–1885

Lundgren MR, Dunning LT, Olofsson JK, Moreno-Villena JJ, Bouvier JW, Sage TL, Khoshravesh R, Sultmanis S, Stata M, Ripley BS, et al (2019) C_4 anatomy can evolve via a single developmental change. Ecol Lett **22:** 302–312

Macfarlane TD (2007) A new species of *Neurachne* (Poaceae) from Western Australia. Nuytsia **17:** 215–222

Maddison WP, Maddison DR (2018) Mesquite: A modular system for evolutionary analysis. Version 3.51 http://www.mesquiteproject.org

Mallmann J, Heckmann D, Bräutigam A, Lercher MJ, Weber AP, Westhoff P, Gowik U (2014) The role of photorespiration during the evolution of C_4 photosynthesis in the genus *Flaveria*. eLife **3:** e02478

McKown AD, Dengler NG (2007) Key innovations in the evolution of Kranz anatomy and C_4 vein pattern in *Flaveria* (Asteraceae). Am J Bot **94:** 382–399

McKown AD, Moncalvo JM, Dengler NG (2005) Phylogeny of *Flaveria* (Asteraceae) and inference of C_4 photosynthesis evolution. Am J Bot **92:** 1911–1928

Monson RK, Edwards GE, Ku MSB (1984) C_3-C_4 intermediate photosynthesis in plants. Bioscience **34:** 563–574

Monson R, Rawsthorne S (2000) CO2 assimilation in C3-C4 intermediate plants. In R Leegood, T Sharkey, and S von Caemmerer, eds, Photosynthesis: Physiology and Metabolism, Vol **Vol 9**. Springer, Dordrecht, pp 533–550

Moore BD, Edwards GE (1989) Metabolism of (CO_2) ^{14}C by leaves of different photosynthetic types of *Neurachne* species. Plant Sci **60:** 155–161

Muhaidat R, Sage TL, Frohlich MW, Dengler NG, Sage RF (2011) Characterization of C_3-C_4 intermediate species in the genus *Heliotropium* L. (Boraginaceae): Anatomy, ultrastructure and enzyme activity. Plant Cell Environ **34:** 1723–1736

Oakley JC, Sultmanis S, Stinson CR, Sage TL, Sage RF (2014) Comparative studies of C_3 and C_4 *Atriplex* hybrids in the genomics era: Physiological assessments. J Exp Bot **65:** 3637–3647

Ogle K (2003) Implications of interveinal distance for quantum yield in C4 grasses: A modeling and meta-analysis. Oecologia **136:** 532–542

Paradis E, Claude J, Strimmer K (2004) APE: Analyses of phylogenetics and evolution in R language. Bioinformatics **20:** 289–290

Prendergast H, Hattersley P (1985) Distribution and cytology of Australian *Neurachne* and its allies (Poaceae), a group containing C_3, C_4 and C_3-C_4 Intermediate species. Aust J Bot **33:** 317–336

Revell LJ (2012) Phytools: An R package for phylogenetic comparative biology (and other things). Methods Ecol Evol **3:** 217–223

Revell LJ (2009) Size-correction and principal components for interspecific comparative studies. Evolution **63:** 3258–3268

Sage RF (2016) A portrait of the C_4 photosynthetic family on the 50th anniversary of its discovery: Species number, evolutionary lineages, and Hall of Fame. J Exp Bot **67:** 4039–4056

Sage RF, Christin PA, Edwards EJ (2011a) The C_4 plant lineages of planet Earth. J Exp Bot **62:** 3155–3169

Sage RF, Khoshravesh R, Sage TL (2014) From proto-Kranz to C_4 Kranz: Building the bridge to C_4 photosynthesis. J Exp Bot **65:** 3341–3356

Sage RF, Sage TL, Kocacinar F (2012) Photorespiration and the evolution of C_4 photosynthesis. Annu Rev Plant Biol **63:** 19–47

Sage TL, Busch FA, Johnson DC, Friesen PC, Stinson CR, Stata M, Sultmanis S, Rahman BA, Rawsthorne S, Sage RF (2013) Initial events during the evolution of C_4 photosynthesis in C_3 species of *Flaveria*. Plant Physiol **163:** 1266–1276

Sage TL, Sage RF, Vogan PJ, Rahman B, Johnson DC, Oakley JC, Heckel MA (2011b) The occurrence of C_2 photosynthesis in *Euphorbia* subgenus Chamaesyce (Euphorbiaceae). J Exp Bot **62:** 3183–3195

Schneider CA, Rasband WS, Eliceiri KW (2012) NIH Image to ImageJ: 25 years of image analysis. Nat Methods **9:** 671–675

Schulze S, Mallmann J, Burscheidt J, Koczor M, Streubel M, Bauwe H, Gowik U, Westhoff P (2013) Evolution of C_4 photosynthesis in the genus *Flaveria*: Establishment of a photorespiratory CO_2 pump. Plant Cell **25:** 2522–2535

Schüssler C, Freitag H, Koteyeva N, Schmidt D, Edwards G, Voznesenskaya E, Kadereit G (2017) Molecular phylogeny and forms of photosynthesis in tribe *Salsoleae* (Chenopodiaceae). J Exp Bot **68:** 207–223

Stata M, Sage TL, Rennie TD, Khoshravesh R, Sultmanis S, Khaikin Y, Ludwig M, Sage RF (2014) Mesophyll cells of C_4 plants have fewer chloroplasts than those of closely related C_3 plants. Plant Cell Environ **37:** 2587–2600

Vogan PJ, Sage RF (2012) Effects of low atmospheric CO_2 and elevated temperature during growth on the gas exchange responses of C_3, C_3-C_4 intermediate, and C_4 species from three evolutionary lineages of C_4 photosynthesis. Oecologia **169:** 341–352

von Caemmerer S (2000) Biochemical Models of Leaf Photosynthesis. CSIRO Publishing, Collingwood, Australia

von Caemmerer S, Furbank RT (2003) The C_4 pathway: An efficient CO_2 pump. Photosynth Res **77:** 191–207

Voznesenskaya EV, Koteyeva NK, Akhani H, Roalson EH, Edwards GE (2013) Structural and physiological analyses in *Salsoleae* (Chenopodiaceae) indicate multiple transitions among C_3, intermediate, and C_4 photosynthesis. J Exp Bot **64:** 3583–3604

Walker BJ, Ort DR (2015) Improved method for measuring the apparent CO_2 photocompensation point resolves the impact of multiple internal conductances to CO_2 to net gas exchange. Plant Cell Environ **38:** 2462–2474

Walker BJ, Skabelund DC, Busch FA, Ort DR (2016) An improved approach for measuring the impact of multiple CO_2 conductances on the apparent photorespiratory CO_2 compensation point through slope-intercept regression. Plant Cell Environ **39:** 1198–1203

Wang P, Khoshravesh R, Karki S, Tapia R, Balahadia CP, Bandyopadhyay A, Quick WP, Furbank R, Sage TL, Langdale JA (2017) Re-creation of a key step in the evolutionary switch from a C_3 to C_4 leaf anatomy. Curr Biol **27:** 3278–3287.e6

Waters MT, Wang P, Korkaric M, Capper RG, Saunders NJ, Langdale JA (2009) GLK transcription factors coordinate expression of the photosynthetic apparatus in *Arabidopsis*. Plant Cell **21:** 1109–1128

Williams BP, Johnston IG, Covshoff S, Hibberd JM (2013) Phenotypic landscape inference reveals multiple evolutionary paths to C_4 photosynthesis. eLife **2:** e00961

Yang Y, Berry PE (2011) Phylogenetics of the Chamaesyce clade (*Euphorbia*, Euphorbiaceae): Reticulate evolution and long-distance dispersal in a prominent C_4 lineage. Am J Bot **98:** 1486–1503